IDENTIFYING STRUCTURAL MISMATCH FOR OPTIMIZATION MODELS

by

JESSE SAENZ, B.S.

A THESIS

IN

CHEMICAL ENGINEERING

Submitted to the Graduate Faculty
of Texas Tech University in
Partial Fulfillment of
the Requirements for
the Degree of

MASTER OF SCIENCE

IN

CHEMICAL ENGINEERING

Approved

James Riggs
Chairperson of the Committee

Karlene Hoo

Accepted

John Borrelli
Dean of the Graduate School

August, 2005

ACKNOWLEDGEMENTS

Every moment in life prepares us for the future and as I look back on all the years I have spent preparing for the future, I realize that I have received help and guidance from countless people. Although I am unable to thank them all, they will remain in my heart forever.

Above all, I owe thanks to my wife, Shellie, and two sons, Nikolas and Justin. They have been my inspiration and I owe them everything. No matter how hard my day was I always looked forward to coming home and seeing my family. They have brought joy to my heart on the worst of days and I am looking forward to being able to spend more time with them. My wife has kept our family going and I will never be able to thank her enough for all she has done, sacrificed, and endured over the years I have been in school.

I would also like to express my sincerest gratitude to Dr. James B. Riggs for allowing me to work on this project. His guidance and support allowed me to complete this project and have prepared me well for my work in the future. It has been a pleasure to have one of the best professors in the department as my advisor and I walk away from this experience with a much greater understanding of optimization as well as many other chemical engineering concepts.

It is an honor to have Dr. Karlene Hoo serve on my committee. Although I was only able to take one course with her as the professor, it was one of my most enjoyable classes and I gained a much greater understanding of process control. Dr. Hoo is one of

the hardest working professors in the department and I have truly enjoyed getting to know her over the past two years.

Jan Hudson and Mary Beth Abernathy also deserve special recognition. They have helped me numerous times with the Process Control and Optimization Consortium as well as any other time I needed their assistance. I truly believe that they hold the department together and we are very lucky to have them.

My fellow students have also been of great help over the years. I feel that I have spent more time with them than with my own family. It has been nice to have people to talk to whenever I needed a break or a different perspective on a problem. I will never forget the long hours we spent on homework and studying for exams, no matter how hard I try.

Of course I would not have accomplished all that I have if it weren't for my parents. They have worked hard my entire life to ensure that I was provided with everything I needed and much more. They raised me to be independent and guided me through life to help me become the person I am today. I can not thank them enough for all they have given me and I hope they know how grateful I am.

TABLE OF CONTENTS

ABSTRACT

Major successes have been achieved with the application of on-line optimization applications particularly real-time optimization (RTO). Although there has been much success with RTO, it has been shown that the performance of an RTO application tends to decrease over time due to changes in the process that are unaccounted for in the optimization models. The main objective of this work is to develop a procedure that can be used in an industrial environment to identify structural model mismatch between the actual process units and the optimization models.

RTO uses complex process models to determine the optimum operating conditions of a process and these models are updated using process measurements so that they provide the most accurate predictions. It is shown in this study that structural model mismatch can be identified by looking at the variation in the calculated model parameters when there are variations in the process operating conditions and sensor noise is not excessive. The effect of model mismatch on calculated model parameters is studied for a heat exchanger, CSTR, distillation column, and an ethylene furnace in this work.

Because RTO applications use process measurements to update model parameters a better measurement should lead to an improvement in the performance of the application. It is shown in this study that decreasing the amount of noise associated with a sensor used by an optimization application leads to a small increase in overall profit, less than 0.4% for the cases considered here, and the increase in profit depends on the shape of the optimization curve about the optimum.

LIST OF TABLES

LIST OF FIGURES

CHAPTER 1

INTRODUCTION

1.1 Optimization in Industry

Optimization in the chemical process industry has become necessary for companies due to increased global competition, operating costs, and tightening product quality constraints (Forbes, 1994). Over the past several decades optimization has evolved from a methodology of academic interest into a technology that has and continues to make a significant impact in industry (Biegler, 2004).

On-line optimization has been shown to yield a significant increase in plant profit for many different applications. On-line optimization has been applied to plants that produce methanol, vinyl acetate monomer, and para-xylene as well as refineries and ethylene plants. Implementations of on-line optimization in the early 1980's through the early 1990's generally had a profitability of about 3% or 4 M$ per year (Lauks, 1992). Applying real-time optimization (RTO) to hydrocarbon-producing systems can increase production rates by as much as 3 to 10% and yield improvement in facility down time (Bybee, 2003).

In today's economy it is no longer enough to simply optimize a single plant or refinery. Companies today must integrate and optimize their overall operations in order to stay competitive. Integrated complexes can exchange over 50 product streams at flow rates of over 100,000 barrels per day. ExxonMobil has surged ahead of its competitors because of tight integration between chemical plants and refineries and their ability to

optimize the integrated process streams (Westervelt, 2004). RTO plays a vital role in the optimization of ExxonMobil's refineries and chemical plants allowing them to continue to increase profits as competitors fall behind (Westervelt, 2004).

1.2 Real-Time Optimization

RTO has become more and more common in the chemical process industry because of improved technology, its ability to estimate the optimum operating conditions of a process accurately, and the increase in profit that can be attained. RTO uses detailed process models to estimate the optimum operating conditions of a process. The optimum operating conditions are found from the model predictions thus, the performance of an RTO application depends greatly on model fidelity.

There are five steps in a typical RTO application. The first step is determining whether or not the process is at steady state. Once steady state is achieved data reconciliation is performed to eliminate any bad process measurements. The third step is model parameterization in which process measurements are used to update the optimization models so that they provide the most accurate predictions. Next, the optimum operating conditions are found using the optimization. The final step is implementation of the setpoints found by the optimizer via an advanced control system. These five steps are continuously implemented.

Computation time, or the time required to find the optimum operating conditions, is a major issue with RTO or any model based optimization application. A typical RTO application will have over 100,000 model equations that must be solved simultaneously

(Rico-Ramirez, 2002). To decrease the required computation time, the models are often simplified decreasing model fidelity. Advancements in technology, primarily computer technology, have allowed for large reductions in the amount of time required to solve an industrial scale optimization problem.

1.3 Motivation and Objectives

Past work and previous implementations of optimization applications have shown that optimization, particularly RTO, can produce a significant increase in plant profit (Lauks, 1992). However, RTO applications can be difficult to maintain resulting in a decrease in performance over time. Physical changes to the process, changes in operating conditions, changes in the economy, and shifting of plant personnel all contribute to the difficulties of maintaining an RTO application.

Industrial RTO applications consist of optimization models for many if not all the units in a chemical plant or refinery. Due to the number and complex nature of the optimization models it can be extremely difficult to determine which models are no longer accurately predicting the behavior of the unit in the plant. The major objective of the work in this study is to develop a procedure that can be used to identify which optimization models in an RTO application need to be modified to account for changes in the process.

In this study, the variation in the model parameters that are calculated to update the optimization models are used to identify structural model mismatch between the optimization model and the actual unit in the plant. The procedure given in this study can

then be used to develop software that can monitor model fidelity by looking at the variation in the calculated model parameters and notify the engineer when a model is no longer accurately representing the unit in the plant.

Another issue considered in this study is the economic value of an improved process measurement. In industry it is often difficult to justify the purchase of a new sensor that is used by an optimization application. In this study, the effect of sensor noise on the overall performance of an optimization application is studied to determine the value of an improved measurement.

1.4 Thesis Organization

The optimization of chemical processes is not a new subject. A literature review is provided in Chapter 2. The methodology used in this study is presented in detail in Chapter 3. Several case studies are conducted to determine the effect of structural model mismatch on the variation of the model parameters and each case is discussed in Chapters 4 to 7. A study is also conducted on the value of an improved measurement and the effects of sensor noise on the performance of the optimization application and this study is discussed in Chapter 8. Lastly, the conclusions and recommendations for future work are presented in Chapter 9.

CHAPTER 2

LITERATURE REVIEW

Edgar, Himmelblau, and Lasdon (2001) is an excellent source on the optimization of chemical processes. The book provides thorough coverage of optimization beginning with the development of optimization models and the formulation of objective functions. Several methods are discussed for the optimization of both one-dimensional and multidimensional problems. The final sections of the book cover applications of optimization and provide many excellent examples.

Biegler and Grossman et al. (2004) provide a thorough discussion on the advancements that have been achieved over the past 25 years in process optimization. This paper covers many search methods that have been studied and developed as well as different types of optimization problems. The main subjects discussed include continuous variable optimization, discrete optimization, dynamic optimization, and optimization under uncertainty.

Process models are commonly used for the optimization of chemical processes because they allow for an estimate of the optimum operating conditions without making changes to the actual process. The open equation-based approach is most often used in process modeling and has been shown to be effective in solving simulation, optimization, parameter estimation and data reconciliation problems, all using a single set of equations (Rico-Ramirez, 2002). Typical chemical process modeling problems will consist of up to 100,000 equations that must be solved simultaneously and when developing these large

models it is difficult not to include structural inconsistencies (Rico-Ramirez, 2002). Rico-Ramirez et al. (2002) proposes that structural analysis is an indispensable tool in an open equation-based modeling environment and provides a procedure that can be used to determine the structural consistency of a model. Structural analysis is a tool applied to exploit sparsity in the solving of a system of equations and structural inconsistencies are detected using an incidence matrix (Rico-Ramirez, 2002).

Sequeira et al. (2002) provides a good introduction to real-time optimization (RTO) as well as an alternative to RTO called real-time evolution (RTE). Typical RTO applications must wait for the process to attain steady state before performing model parameterization, finding the optimum operating conditions and then moving the process to the new optimum via an advanced control system. RTE, however, does not have to wait for the process to reach steady state to begin moving the process towards a new optimum (Sequiera, 2002). When a disturbance is measured RTE will calculate a new optimum and begin to move the process towards the new optimum even if the process is not at steady state. RTE uses disturbance measurements, current setpoints, and rigorous models to find the new optimum during transient periods (Sequeira, 2002). RTE can be more effective than typical RTO because the optimum operating conditions will change over time due to changes in the process and changes in market conditions.

Singh et al. (2000) provides an excellent example of a typical industrial RTO application. Model-based RTO is applied to the gasoline blending operations of a typical refinery. This study provides a detailed analysis of the optimization models as well as product specifications. Typical RTO has been found to be effective when feedstocks to

the blending process originate from "standing" tanks, however, typical RTO can be less effective when in-line blending or blending from "running" tanks is performed due to upstream process disturbances (Singh, 2000). Upstream process disturbances are absorbed in the "standing" tanks providing constant feedstock properties. When in-line blending or blending from "running" tanks is performed feedstock properties may vary over time due to upstream disturbances. Singh et al. (2000) proposes the use of time horizon based RTO (THRTO) for this application which differs from typical RTO in that the blend horizon is discretized and divided into two parts (past and future). Then, optimization occurs only over the remaining blending time interval between the current time and the blend completion time (Singh, 2000). A case study is performed to compare the performance of three blend optimization strategies: (1) the conventional linear programming with bias update approach; (2) a nonlinear programming with bias update approach; and (3) the THRTO approach (Singh, 2000).

Forbes, Marlin, and MacGregor et al. (1994) propose a means for evaluating candidate process models and selecting those which are adequate for operations optimization. This study shows that, although it may be useful for monitoring plant performance, it is not necessary for an optimization application to predict the actual value of profit attained but that is must merely accurately predict the manipulated variable values that coincide with the values of the true process optimum (Forbes, 1994). The proposed methods in this study use a point-wise model adequacy criterion that will allow an optimization system designer to investigate the suitability of a process model for use in an optimization system prior to implementation (Forbes, 1994).

Yip and Marlin et al. (2004) have studied the effect of model fidelity on RTO performance. Three types of optimization applications are considered in this study applied to a boiler network: (1) model-free direct search methods that track the optimum based on plant data without using a detailed model; (2) model-based method using a simplified model; (3) model-based method using a fundamental model (Yip, 2004). It is found in this study that using the model-based method with the fundamental model allowed for better tracking of the optimum operating conditions when compared to the other two options (Yip, 2004). The model free direct search method as well as the model based method using a simplified model both require process experimentation to determine the optimum operating conditions leading to lost profit while experimentation is being performed (Yip, 2004).

Uncertainty is an inherent characteristic in RTO applications and is caused by market uncertainty, measurement uncertainty, and model uncertainty (Zhang, 2002). Zhang et al. (2002) proposes a stochastic optimization approach to robust RTO that deals effectively with parametric uncertainty. The approach taken in this work is to address uncertainty with the probability of constraint violation (Zhang, 2002). The proposed stochastic optimization approach is applied to a gas blending process and compared to the performance of a typical RTO application. It is found that using the approach proposed by Zhang et al. (2002) leads to a large decrease in the number of times that a constraint is violated. The computation time of the proposed approach was found to be an order of magnitude larger than that of the typical RTO application but the improved performance will most likely justify its use (Zhang, 2002).

In RTO applications feedback data used to update model parameters includes noise and the effects of high-frequency disturbances resulting in optimization calculations that are corrupted by a stochastic component (Milectic, 1998). Milectic and Marlin et al. (1998) propose an on-line statistical results analysis that greatly reduces the number of unnecessary RTO moves caused by noise and high frequency disturbances. The performance of an RTO application using the proposed statistical analysis was compared to that of a typical RTO application and it was found that using the proposed statistical analysis lead to an increase in overall plant profit (Milectic, 1998).

Krishnan et al. (1992) proposes a method to identify sensor readings that will lead to the best performance of an on-line optimization application. The methodology presented in this paper is a two-stage one, determining first the key uncertain model parameters and then a best set of measurements to estimate these parameters. The key model parameters are chosen on the basis of their effect on the calculated optimum (Krishnan, 2002). The best set of measurements used to parameterize the optimization model are found by using a singular value analysis-based technique and it is shown in the case study conducted by Krishnan et al. (1992) that using the best set of process measurements in the on-line optimization application decreases the effect of both sensor noise and inaccurate optimization models on the calculated optimum.

Fraleigh et al. (2002) proposes a systematic approach to the selection of sensor systems to be used by an RTO application. The objective of this approach is to choose the sensor system design that has the least bias in the setpoint predictions generated for the RTO design basis (Fraleigh, 2002). The sensor system selection procedure takes into

account the capital cost of the sensor system designs as well as the observability of the adjustable parameters. The Williams-Otto plant is studied in the work done by Fraleigh et al. (2002), and it is shown that the profit attained using RTO can be increased by 15% using the proposed procedure to determine the optimal location of a composition analyzer.

In industry it is often difficult to justify, economically, the installation of more accurate sensors in a plant or refinery. Bagajewicz et al. (2003), proposes a connection between precision and expected lost revenue for linear systems that can be used to determine the Net Present Value (NPV) of a more accurate reading as well as the installation of a data reconciliation package. All sensor network properties (precision, residual precision, error detectability, reliability and resilience) are related to lost or increased revenue functions converting the problem into an unconstrained one based on cost-benefit only (Bagajewicz, 2003). Lost and increased revenue is based on the probability of failing to meet or exceed production needs based on sensor readings (Bagajewicz, 2003).

CHAPTER 3

METHODOLOGY

Process modeling plays a vital role in the optimization of chemical processes in the chemical process industry. Process models are generally a complex set of algebraic and differential equations that can be solved on a computer. These models are used to predict the response of a unit to changes in the operating conditions and this prediction allows for the optimum operating conditions to be estimated without making changes to the actual process. The process models used to represent the optimization models are referred to through out this study as "approximate models."

In industrial optimization applications, process data are used to parameterize the optimization models so that they provide the most accurate predictions. In the studies conducted here we do not have access to actual process data so we must develop a process model that is used to represent the actual process. The model used to represent the actual process is referred to through out this study as the "process model" and is used to generate process data.

In industrial optimization applications data reconciliation is used to eliminate bad process data from the model parameterization process. This bad data can come from calibrated sensors, sensor noise, and malfunctioning sensors. It is assumed for all studies conducted here that data reconciliation has been performed before the sensor readings are sent to the approximate model so that the data are free of gross errors. Thus, in this

study, only sensor noise is added to the process measurements predicted by the process model.

Sensor noise is random errors between the measurement and the true process value that does not correspond to real process changes. Each time a model parameter is determined, a different value of the parameter is attained due to the variation in the noise on the process measurement. Monte Carlo simulations are used in this study to determine the effect of random variables on the variance of calculated model parameters and the calculated optimum operating conditions in a chemical process. The term Monte Carlo simulation refers to a stochastic method in which a large number of cases are studied to determine the distribution in the model parameters due to the variation in the measurement. Each simulation uses a different random value for the noise on the measurement leading to variations in the calculated model parameters.

3.1 Determining the Effect of Sensor Noise

Sensor noise is the variation in the sensor reading that does not correspond to changes in the process. Sensor noise can be caused by background electrical interference and mechanical vibrations (Riggs, 2001). There are different amounts of sensor noise associated with different types of sensors and the amount of noise associated with a properly functioning sensor is directly related to the repeatability of the sensor. For example, a properly functioning thermocouple has a repeatability of ±1ºC meaning that the sensor reading will vary by ±1ºC around the true value most of the time.

When process data is used to parameterize an optimization model, sensor noise is included in the data. Variations due to sensor noise in the process data can lead to variations in the model parameters calculated from the process data. The goal here is to determine how the distribution of values of the model parameters is related to the noise level on the process measurements. The effect of sensor noise on the parameterization of the approximate models for a heat exchanger, CSTR, distillation column and an ethylene furnace is investigated in this work.

The general procedure used to determine the effect of sensor noise on the model parameters calculated from process data is the same for all of the units considered in this study. Process measurements are generated by the process model and then sensor noise is added to the exact values. The data containing sensor noise are then used to parameterize the approximate model and Monte Carlo simulations are used to determine the resulting variation in model parameters.

The first step is to create a process model of the unit being considered which will be used to represent the actual process. This model is developed using equations and assumptions that are known to model the unit accurately and this is discussed in detail in the following chapters.

The process operating conditions are generated by the process model and sensor noise is then added to these exact values producing process measurements. Although sensor noise may be more complex, in this study it is assumed to be Gaussian-distributed white noise and is modeled using a random number generator. When Matlab is used to run the trials the Matlab function RANDN is used to generate the sensor noise with the

desired distribution. When Fortran is used to run the trials a subroutine was written using an equation to model Gaussian-distributed white noise (Riggs, 2001). The desired amount of noise is obtained by specifying the standard deviation, σ, of the numbers generated by the random number generator where 4σ (i.e., $\pm 2\sigma$) should contain 95% of the sensor readings (Riggs, 2001). The standard deviation for each of the sensors is set equal to one half the repeatability for a properly functioning sensor (Riggs, 2001).

These simulated process measurements are used to calculate the model parameters for the corresponding approximate model. At this point, a perfect approximate model is assumed so that the variation in the calculated model parameters due solely to sensor noise can be determined.

Monte Carlo simulations are then used to determine the variance in the model parameters caused by sensor noise. A statistical analysis can be performed on the data generated by the Monte Carlo simulations to quantify the variation in the model parameter or a histogram can be plotted to visualize the variation in the model parameter.

3.2 Determining the Effect of Model Mismatch

Due to the complex nature of chemical processes it is impossible to develop a perfect model. There are many unknown quantities in a chemical process that can not be accounted for in the model, such as feed impurities and unmeasured disturbances. In addition, some times when a highly accurate model is available it must be simplified so that it can be solved within a reasonable amount of time. Unknown quantities and model simplification lead to structural mismatch between the model and the actual process

decreasing the model fidelity or accuracy. The performance of an industrial optimization application depends greatly on the ability of the model to predict changes in the process resulting from input changes accurately. Our goal here is to determine how the distribution of the calculated model parameters is related to the fidelity of the approximate model. The performance of optimization models for a heat exchanger, CSTR, distillation column, and ethylene furnace are investigated in this work.

The procedure used for determining the effect of model mismatch on the parameters calculated from process data is basically the same as that used to determine the effect of sensor noise on model parameters. The only difference is that the approximate model is no longer the same as the process model. The approximate model is now modified to include some type of structural model mismatch. Different degrees of model mismatch are studied to compare how the variation of the model parameter is effected by the degree of model mismatch. The Monte Carlo simulations use sensor noise associated with sensors that have a small repeatability so that the variation caused by model mismatch can be seen clearly.

The inlet conditions to the process model are also varied in the Monte Carlo simulations to represent changes in the operating conditions of the unit. Varying the operating conditions is important in this work because if there are no variations in the operating conditions of the process model there will be no variations in the calculated model parameters other than that caused by sensor noise. For example, if the feed rate and operating temperature of a CSTR are kept constant, the outlet conditions will always be the same resulting in the same calculated model parameters regardless of the degree of

mismatch. When the feed rate and operating temperature of a CSTR are varied, the outlet conditions will vary but the rate constants used in the kinetic equations remain the same. The variation in the outlet conditions leads to variations in the calculated model parameters when structural model mismatch is present. Therefore, the variation in the calculated model parameters is dependent on the variation of the operating conditions as well as the degree of structural model mismatch.

3.3 Determining the Value of an Improved Measurement

The amount of noise on a process reading can usually be reduced by replacing the sensor with a newer sensor or different type of sensor. The question is whether the cost of the new sensor results in significant economic improvement of the optimization application.

The procedure used to determine the value of an improved measurement also requires the use of a process model and an approximate model. Because we are interested only in the value of an improved measurement the approximate model is assumed to be the same as the process model, i.e., there is no mismatch. The value of the measurement is determined by comparing the sum of the profit attained for each trial using different amounts of sensor noise. This requires that an objective function be developed that accounts for feed costs, utility costs, and product values.

The process model is used to generate actual operating conditions and then senor noise is added to the exact process measurements using Gaussian-distributed white noise. The sensor readings for both inlet and outlet conditions are then used to parameterize the

approximate model. The model parameters calculated from process data are used in the approximate model to determine the operating conditions that yield the most profit based on the objective function. The calculated optimum operating conditions and the objective function are then used with the process model to determine the true profit at those conditions.

Monte Carlo simulations are used to determine the overall performance based on process measurements with noise. Histograms can be used to visualize the distribution of the true profit attained and since the same number of simulations is used for each level of sensor noise, the sum of the profit attained for all the simulations can be used to characterize the overall performance. The effect of sensor noise on the total profit attained by optimizing the process operating conditions is evaluated for a CSTR, distillation column, and an ethylene furnace in this work.

CHAPTER 4

HEAT EXCHANGER STUDY

Heat exchangers are used throughout the chemical process industry to transfer heat from one process stream to another and also to maintain the desired operating temperature of a unit. They play a vital role in energy conservation and in the optimization of chemical processes. It is common for a process stream to leave a unit and have either more or less energy than is required. Heat exchangers are used to conserve energy by transferring excess energy to where it is needed. As an example, the flue gas from an ethylene furnace is used to preheat the feed to the furnace so that less fuel is required to achieve the desired results. Instead of wasting the excess energy that is in the flue gas, some of this energy is transferred to the feed reducing the overall fuel cost.

A heat exchanger is the simplest unit considered here and although this unit is not difficult to model it is still of great importance when optimizing a chemical process. As an example, when optimizing a boiler network, heat exchanger fouling can change the shape of the boiler efficiency curve (Marlin & Yip, 2004) having a significant effect on the optimal operating conditions. Fouling in a heat exchanger is common and is caused by build up on the heat exchanger tubes. Fouling will increase over time causing the overall heat transfer coefficient to decrease. Due to the large amounts of heat transfer that can take place in a heat exchanger, heat loss to the surroundings is another factor that must be considered. Neglecting to update the heat exchanger model to account for fouling and heat loss to the surroundings leads to structural mismatch between the

process and the approximate model. Structural mismatch between the process and the approximate heat exchanger model can lead to inaccurate solutions for the optimal operating conditions. This study shows the effect of model mismatch and sensor noise on the variation of the overall heat transfer coefficient calculated from process data.

4.1 Heat Exchanger Model

The macroscopic equation used to model a shell and tube heat exchanger is as follows (Incropera, 2002):

$$Q = \dot{m} C_p \left(T_{h,i} - T_{h,o}\right) = UA\Delta T_{lm} \tag{4.1}$$

where Q is the total heat transferred from the hot stream to the cold stream, $\dot{m}$ is the mass flow rate of the hot stream, C_p is the average heat capacity of the hot stream, $T_{h,i}$ and $T_{h,o}$ are the inlet and outlet temperatures of the hot stream respectively, U is the overall heat transfer coefficient, A is total area of heat transfer, and ΔT_{lm} is the log mean temperature difference. This equation can be solved for U yielding the following result:

$$U = \frac{\dot{m} C_p \left(T_{h,i} - T_{h,o}\right)}{A\Delta T_{lm}}. \tag{4.2}$$

The equation for the log mean temperature difference is as follows:

$$\Delta T_{lm} = \frac{\left(T_{h,o} - T_{c,o}\right) - \left(T_{h,i} - T_{c,i}\right)}{\ln\left(\frac{T_{h,o} - T_{c,o}}{T_{h,i} - T_{c,i}}\right)} \tag{4.3}$$

where $T_{c,o}$ and $T_{c,i}$ are the outlet and inlet temperatures of the cold stream respectively.

The heat capacity of the hot stream is assumed to have a constant value of 2,350 Joules per kilogram and the area of heat transfer is assumed to be 29.77 square meters for all simulations conducted in this chapter.

4.2 Model Mismatch

Model mismatch for the heat exchanger considered here is modeled by heat loss to the surroundings which is not accounted for in the approximate model. To include heat loss to the surroundings in the process model the model equation is modified as follows:

$$Q = \dot{m} C_p \left(T_{h,i} - T_{h,o}\right) - Q_{loss} = UA\Delta T_{lm} \tag{4.4}$$

where Q_{loss} represents heat loss to the surroundings and is specified as a percentage of the total heat transferred. This equation is again solved for U yielding the following result:

$$U = \frac{\dot{m} C_p \left(T_{h,i} - T_{h,o}\right) - Q_{loss}}{A\Delta T_{lm}}. \tag{4.5}$$

The process model, which accounts for heat loss to the surroundings, is used to generate the process data that are used to parameterize the approximate model.

4.3 Results

There are five process measurements used to parameterize the approximate heat exchanger model, four temperature measurements and one flow measurement. The temperature sensors are assumed to be either thermocouples or RTDs with a repeatability of ±1.0ºC or ±0.1ºC respectively (Riggs, 2001). The flow meter is assumed to be an

orifice flow meter with a repeatability of ±0.3% (Riggs, 2001) for all trials. The variation in the overall heat transfer coefficient was generated using 10,000 simulations.

When looking only at the effect of sensor noise on the calculated overall heat transfer coefficient, U, it can be seen in Figure 4.1 that reducing the amount of sensor noise greatly reduces the variance in the overall heat transfer coefficient. The standard deviation of the overall heat transfer coefficient for thermocouples increases by a factor of ten when compared to the standard deviation when using RTDs. This result is expected because the sensor repeatability also increases by a factor of ten when comparing thermocouples to RTDs. The standard deviations of these results are given in Table 4.1.

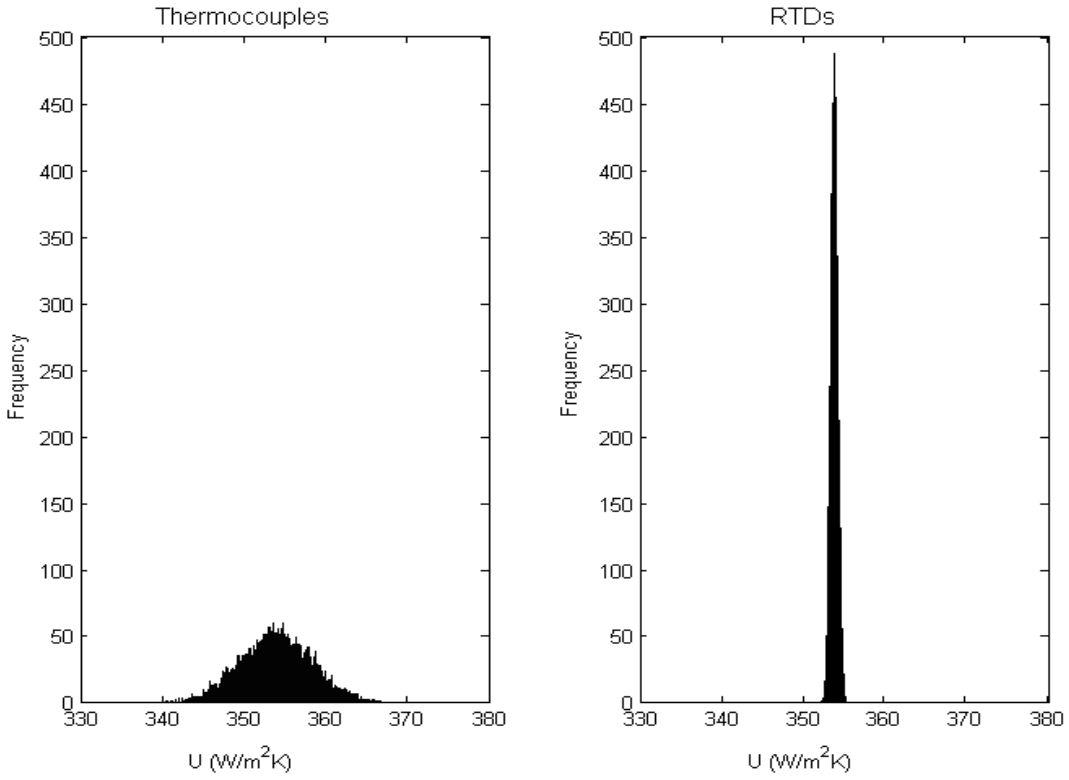

Figure 4.1. The effect of sensor noise on the variance of the overall heat transfer coefficient.

Adding structural model mismatch significantly increases the variance in the overall heat transfer coefficient as can be seen in Figure 4.2. The data in Figure 4.2 was generated using sensor noise associated with properly functioning RTDs. It can be seen that when there is 0% heat loss, i.e., a perfect model, the variance in U is that caused solely by sensor noise. As the percentage of heat loss to the surroundings is increased to 5 and 10%, the variance also increases showing that as model mismatch is increased so is the variance. Another result of increasing the percentage of heat loss to the surroundings is that the average calculated value of the overall heat transfer coefficient decreases. This is a result of less heat being transferred from the hot stream to the cold stream as heat loss to the surroundings is increased.

Table 4.1: Standard deviation of U (W/m^2K) caused by sensor noise.

Model Parameter	RTDs	Thermocouples
U (W/m^2K)	0.43	4.31

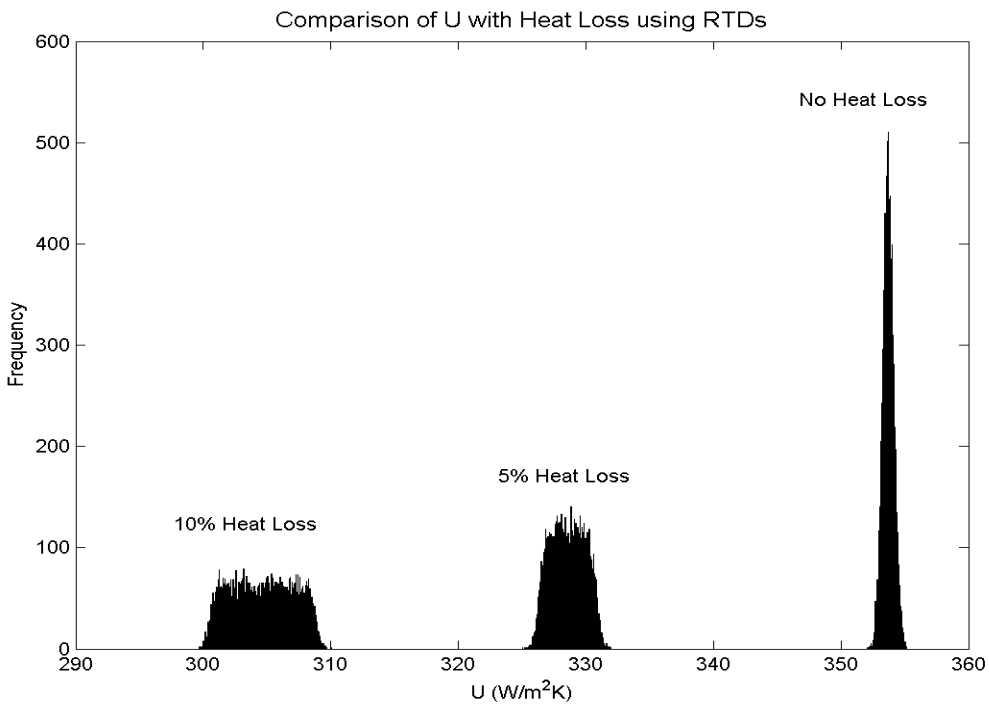

Figure 4.2. The effect of model mismatch on the variance of the overall heat transfer coefficient when RTDs are used.

It can be seen in Figure 4.3 that when using sensor noise associated with properly functioning thermocouples, there is not a significant increase in the variance of the overall heat transfer coefficient as heat loss to the surroundings is increased. The variance in the calculated overall heat transfer coefficient does not increase for this particular application because the variation caused by the large amounts of sensor noise outweighs the variation caused by model mismatch.

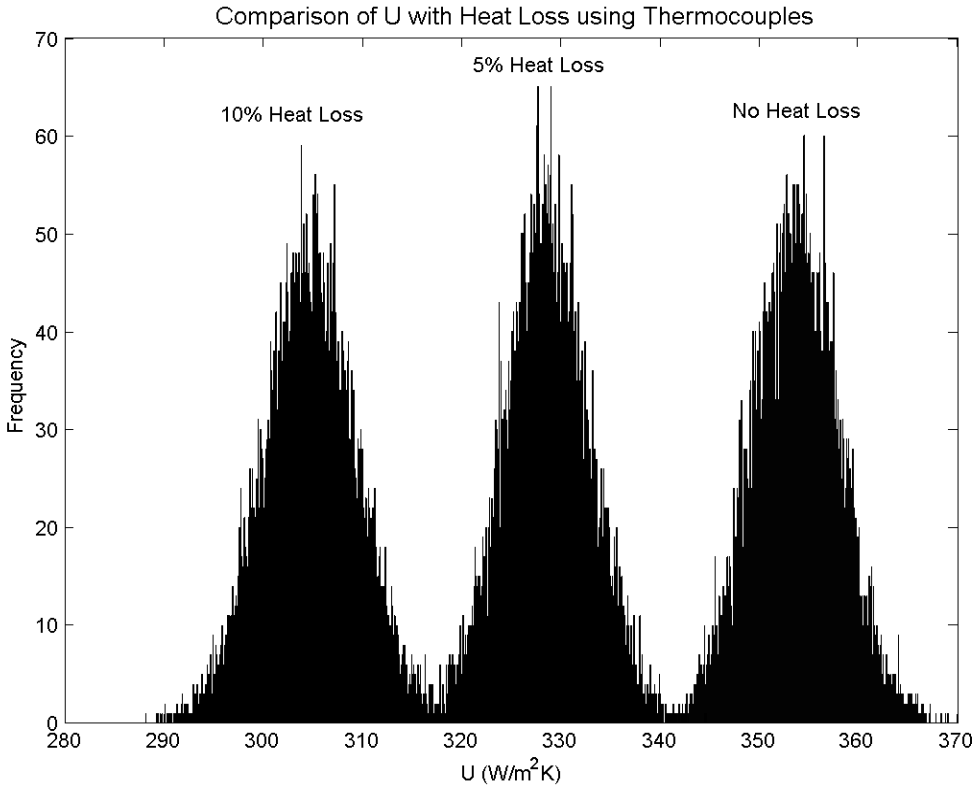

Figure 4.3. The effect of model mismatch on the variance of the overall heat transfer coefficient when thermocouples are used.

It can be seen from the results provided in this chapter that for this particular case structural mismatch in the approximate model can be identified by looking at the distribution of the overall heat transfer coefficient when RTDs are used. As the structural mismatch in the approximate model is increased, so is the observed variation in the overall heat transfer coefficient. When thermocouples are used, it is not possible to identify structural mismatch in the approximate model due to the magnitude of sensor noise. The standard deviations of these results are given in Table 4.2.

Table 4.2: Standard deviation of U (W/m^2K) caused by mismatch.

Sensors	0% Heat Loss	5% Heat Loss	10% Heat Loss
RTDs	0.43	1.32	2.42
Thermocouples	4.31	4.23	4.58

CHAPTER 5

CSTR STUDY

Continuously stirred tank reactors (CSTRs) are common in the chemical process industry because they are useful for both gas and liquid phase reactions and are ideal for continuous processes. CSTRs are used in the production of specialty chemicals, polymers, and in biological processes.

Reactors are usually at the core of a chemical plant, thus optimizing the operating conditions of reactors is vital to the overall optimization of the plant. Reactor models are usually difficult to develop because the performance of a reactor can be influenced by temperature, pressure, species concentration, and feed impurities.

Structural mismatch between the optimization model and the actual process can come in many different forms for a CSTR. The reaction scheme in an industrial reactor is usually very complex making it difficult to model accurately. Structural model mismatch can be caused by incorrect reaction kinetics and invalid assumptions such as perfect mixing in the reactor.

5.1 CSTR Model

There are two under lying assumptions made in the model of a CSTR used in this study:

1) There is perfect mixing.

2) The temperature, pressure, and concentrations throughout the reactor are uniform.

Because the assumption of perfect mixing is made, the temperature and composition in the reactor outlet are the same as in the reactor itself. Although these assumptions are never completely correct, they do allow for a reasonable model of a CSTR. For these assumptions to hold, the reactor must be well mixed.

The CSTR model chosen here is based on the method proposed by Mann (1999). The concentration of each species in the product stream is calculated by using the dimensionless extent of the reactions. The dimensionless extent of reaction m is given as:

$$Z_m = \frac{\dot{X}_m}{(F_{tot})_0} \tag{5.1}$$

where $\dot{X}_m$ is the extent of reaction m and $(F_{tot})_0$ is the total molar feed rate to the reactor. The extent of each reaction leaving the reactor is calculated with the following equation when there are no dependent reactions:

$$Z_m = r_m \tau \left(\frac{t_{cr}}{C_0} \right) + Z_{m,in} \tag{5.2}$$

where Z_m and $Z_{m,in}$ are the dimensionless extents of reaction m at the reactor outlet and inlet respectively, r_m is the rate of reaction m, τ is the dimensionless space time, t_{cr} is the characteristic reaction time, and C_0 is the characteristic concentration. The rate of each of the reactions is assumed to have the following form:

$$r = k(T)C_i^{\alpha}C_j^{\beta} \tag{5.3}$$

where $k(T)$ is the reaction rate constant which is a function of temperature, C_i and C_j are the concentrations of reactants i and j respectively, and α and β are the order of species i and j respectively. The reaction rate constant is assumed to have Arrhenius temperature dependence and is given as:

$$k(T) = k_0 \exp\left(-\frac{E_a}{RT}\right) \tag{5.4}$$

where k_0 is the frequency factor, E_a is the activation energy, R is the gas constant, and T is temperature. The dimensionless space time for a CSTR is defined as:

$$\tau \equiv \frac{V_R}{v_0 t_{cr}} \tag{5.5}$$

where V_R is the reactor volume and v_0 is the volumetric feed rate. The characteristic reaction time is given as:

$$t_{cr} = \frac{C_0}{r_0} \tag{5.6}$$

where r_0 is the characteristic reaction rate. The characteristic concentration is given as:

$$C_0 = \frac{(F_{tot})_0}{v_0}. \tag{5.7}$$

The concentration of each species exiting the reactor is a function of the dimensionless extent of each reaction and can be calculated with the following equation:

$$C_j = C_0\left(y_{j0} + \sum_{m}^{n_{ind}} s_{j,m} Z_m\right) \tag{5.8}$$

where C_j is the concentration of species j in the reactor, y_{j0} is the mol fraction of species j in the feed, n_{ind} is the number of independent reactions, and $s_{j,m}$ is the stoichiometric coefficient of species j in reaction m.

The base case reaction scheme is assumed to have two reactions taking place and they are as follows:

Reaction 1: $A + B \rightarrow V$

Reaction 2: $V + B \rightarrow W$

Each of the reactions are assumed to be first order with respect to each of the reactants, i.e., second order overall, and the reactor is operated isothermally. There are two feed streams to the reactor, one containing reactant A and the other containing reactant B. Equation (5.2) is used to solve for the dimensionless extent of each reaction and the equations are as follows:

$$Z_1 = k_{1,0} \exp\left(-\frac{E_{a,1}}{RT}\right) C_0 \left(y_{A0} + s_{A,1} Z_1\right)\left(y_{B0} + s_{B,1} Z_1 + s_{B,2} Z_2\right) \frac{V_R}{v_0} \tag{5.9}$$

$$Z_2 = k_{2,0} \exp\left(-\frac{E_{a,2}}{RT}\right) C_0 \left(y_{V0} + s_{V,1} Z_1 + s_{V,2} Z_2\right)\left(y_{B0} + s_{B,1} Z_1 + s_{B,2} Z_2\right) \frac{V_R}{v_0} \tag{5.10}$$

where $Z_{1,in}$ and $Z_{2,in}$ are both zero. Equations (5.9) and (5.10) are solved simultaneously using the Newton-Raphson Method for Simultaneous Non-Linear Equations (Rao, 2002). Using the values of Z_1 and Z_2, Equation (5.8) is used to solve for the exit concentration of each species in the reactor.

Table 5.1 provides the constant values of parameters used in the base case CSTR model.

Table 5.1: Base case CSTR data.

V_R	500 $(liters)$
$k_{1,0}$	0.8 $\left(liters/mol \cdot \min\right)$
$k_{2,0}$	0.7 $\left(liters/mol \cdot \min\right)$
$E_{a,1}$	12,000 $\left(cal/mol\right)$
$E_{a,2}$	15,000 $\left(cal/mol\right)$

5.2 Model Mismatch

The first type of model mismatch is an error in the activation energies of the reactions. The process model remains the same as that used in the base case but the activation energies in the approximate model are now assumed to be a certain percentage of those used in the process model.

The second type of model mismatch considered here is a different reaction scheme for the process model. Reaction 2 in the base case is assumed to be reversible in the process model and this is neglected in the approximate model. The reaction scheme used in the process model is now:

$$\text{Reaction 1:} \quad A + B \rightarrow V$$

$$\text{Reaction 2:} \quad V + B \leftrightarrow W \ .$$

This type of model mismatch is most likely be difficult to identify because there are no additional products produced and the frequency factor in the backward reaction is assumed to be 10% of the value used in the forward reaction, i.e., the backward reaction rate is slower than that of the forward reaction.

The third and final type of model mismatch is a different reaction rate equation in the process model than used in the approximate model. In the approximate model, the terms α and β are assumed to be equal to one for each reaction as in the base case. However, in the process model α and β are assumed to have a value other than one leading to structural mismatch between the process model and the approximate model.

5.3 Results

There are three process measurements used to parameterize the approximate CSTR model, one temperature measurement, one flow measurement, and a composition analyzer. The temperature sensor is assumed to be either a thermocouple or an RTD and the flow meter is assumed to be either an orifice flow meter or a magnetic flow meter with a repeatability of ±0.3% or ±0.1% respectively. The repeatability of the composition analyzer is set equal to ±1% or ±10% for the desired noise level. The variation in the frequency factor for each of the reactions was generated using 10,000 Monte Carlo simulations.

When looking at the effect of sensor noise on the variation in the calculated frequency factor for each of the reactions, it can be seen in Figures 5.1 and 5.2 that reducing the amount of sensor noise significantly reduces the variance in the frequency factors. A small amount of noise corresponds to the use of an RTD, magnetic flow meter, and ±1% repeatability on the composition analyzer. A large amount of noise corresponds to the use of a thermocouple, orifice flow meter, and ±10% repeatability on

the composition analyzer. The standard deviations of these results are provided in Table 5.2.

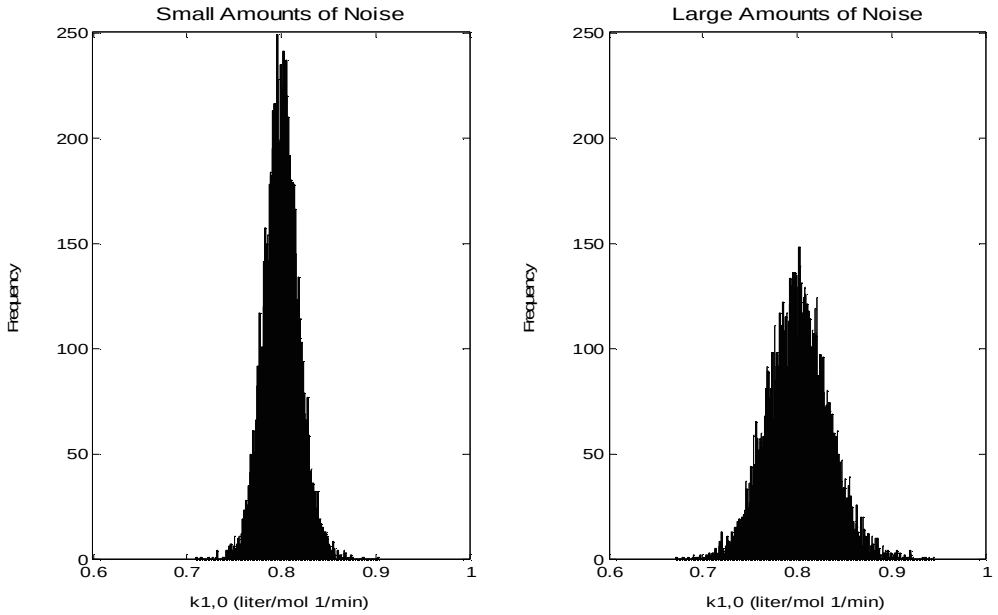

Figure 5.1. The effect of sensor noise on the variance of $k_{1,0}$.

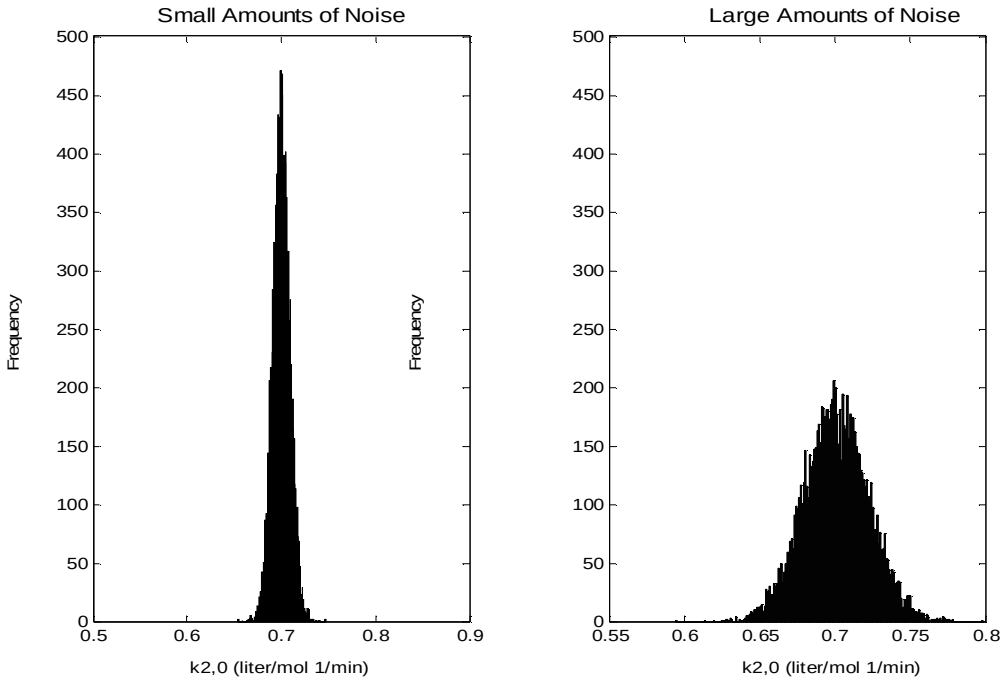

Figure 5.2. The effect of sensor noise on the variance of $k_{2,0}$.

Table 5.2: Standard deviation of frequency factors caused by sensor noise.

Noise	$k_{1,0}$ (liter/mol·min)	$k_{2,0}$ (liter/mol·min)
Small Amount	0.02	0.01
Large Amount	0.20	0.11

For the first type of model mismatch it can be seen in Figures 5.3 and 5.4 that as the percent error in the activation energy is increased, the variance in the calculated frequency factors also increases. When the error in the activation energy is 0%, i.e., a perfect model, the variation is that caused solely by sensor noise.

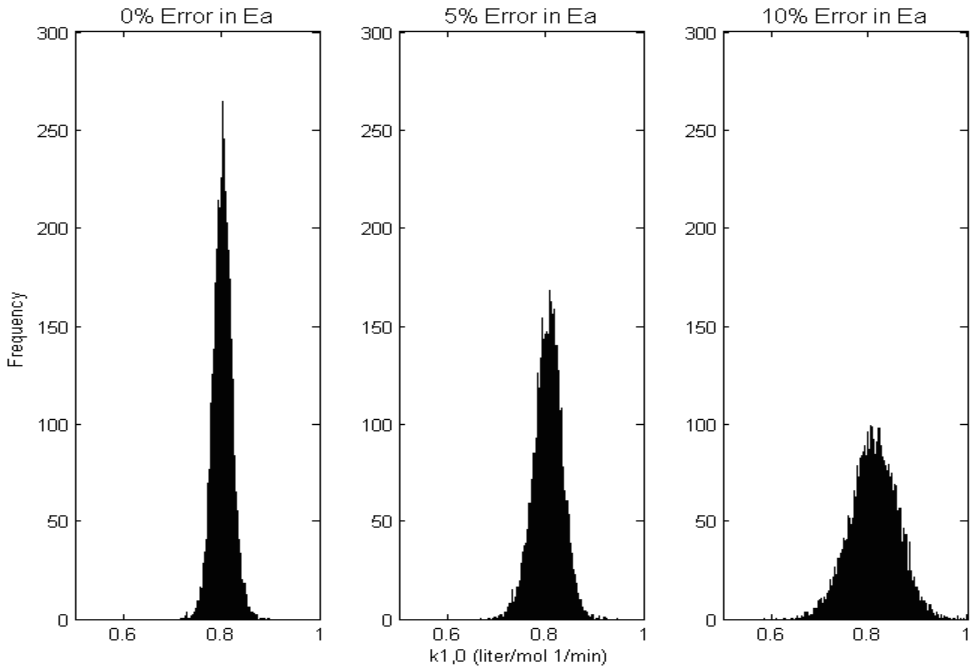

Figure 5.3. The effect of an error in the activation energy on the variance of $k_{1,0}$ when a small amount of sensor noise is used.

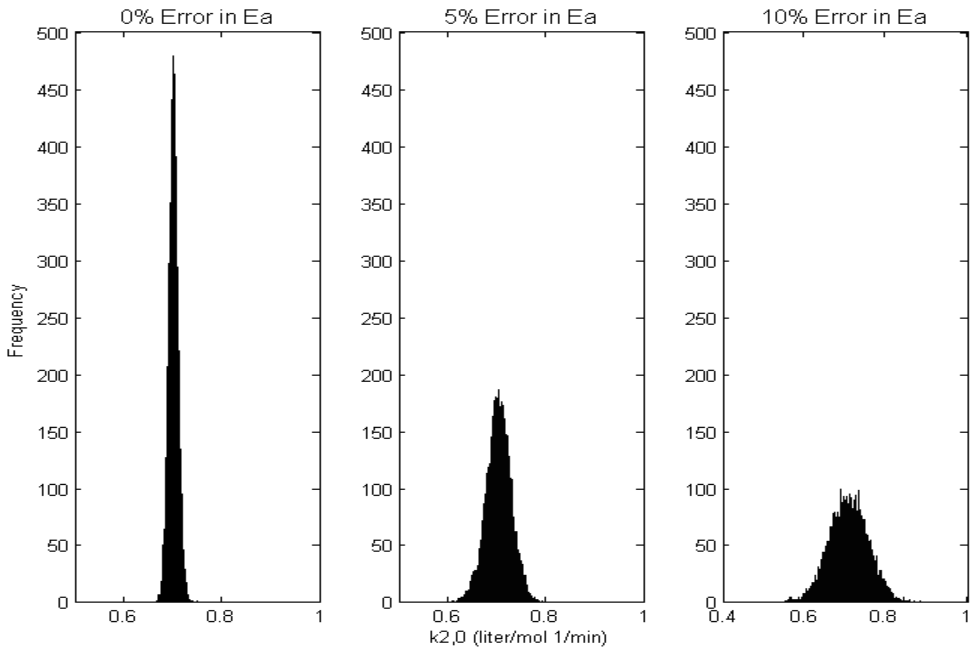

Figure 5.4. The effect of an error in the activation energy on the variance of $k_{2,0}$ when a small amount of sensor noise is used.

When a large amount of sensor noise is used, it is not possible to identify structural mismatch due to errors in the activation energy as can be seen in Figure 5.5. This result was the same for both $k_{1,0}$ and $k_{2,0}$ and is a result of the variation caused by sensor noise outweighing the variation caused by this type of model mismatch. The standard deviations of these results are provided in Tables 5.3 and 5.4.

Table 5.3: Standard deviation of $k_{1,0}$ (liter/mol·min) cased by activation energy errors.

Noise	0% Error	5% Error	10% Error
Small Amount	0.02	0.03	0.05
Large Amount	0.20	0.20	0.20

Table 5.4: Standard deviation of $k_{2,0}$ (liter/mol·min) caused by activation energy errors.

Noise	0% Error	5% Error	10% Error
Small Amount	0.01	0.03	0.05
Large Amount	0.19	0.16	0.15

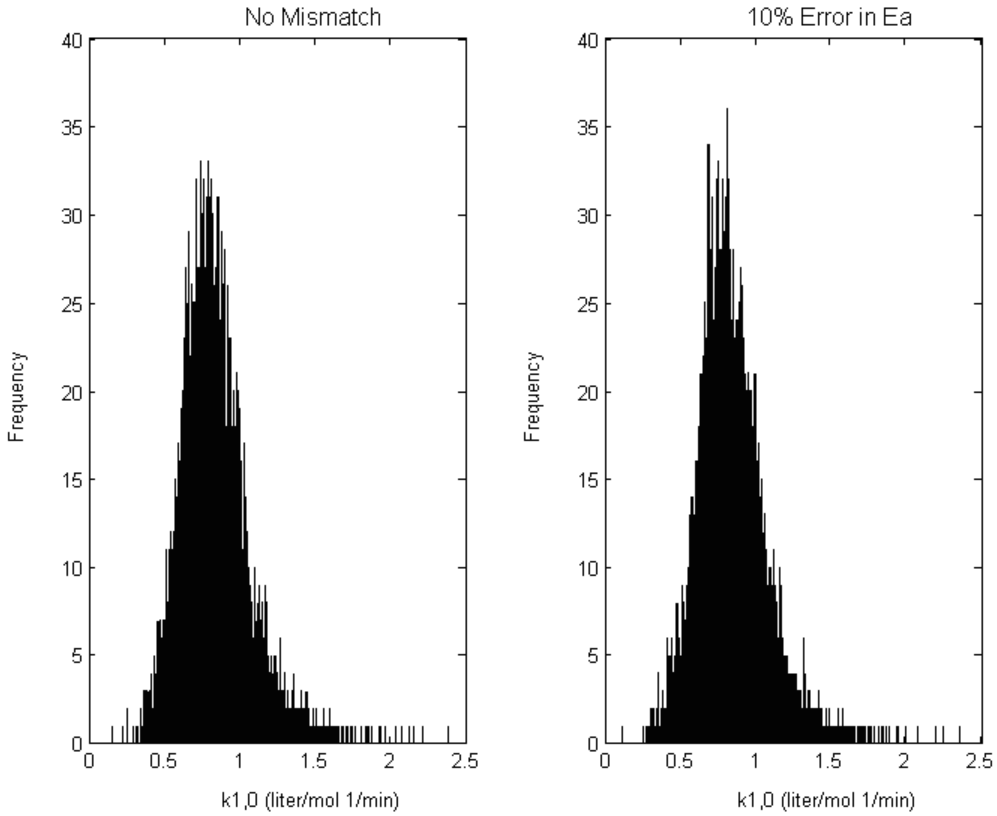

Figure 5.5. The effect of an error in the activation energy on the variance of $k_{1,0}$ when a large amount of sensor noise is used.

For the second type of model mismatch the process model accounts the reversible reaction while the approximate model does not. It can be seen in Figures 5.6 and 5.7 that this type of model mismatch also leads to an increase in the variance of the frequency factors. The variation of both frequency factors increases although only reaction 2 in the base case is considered to be reversible in the process model. The standard deviations of these results are provided in Tables 5.5 and 5.6.

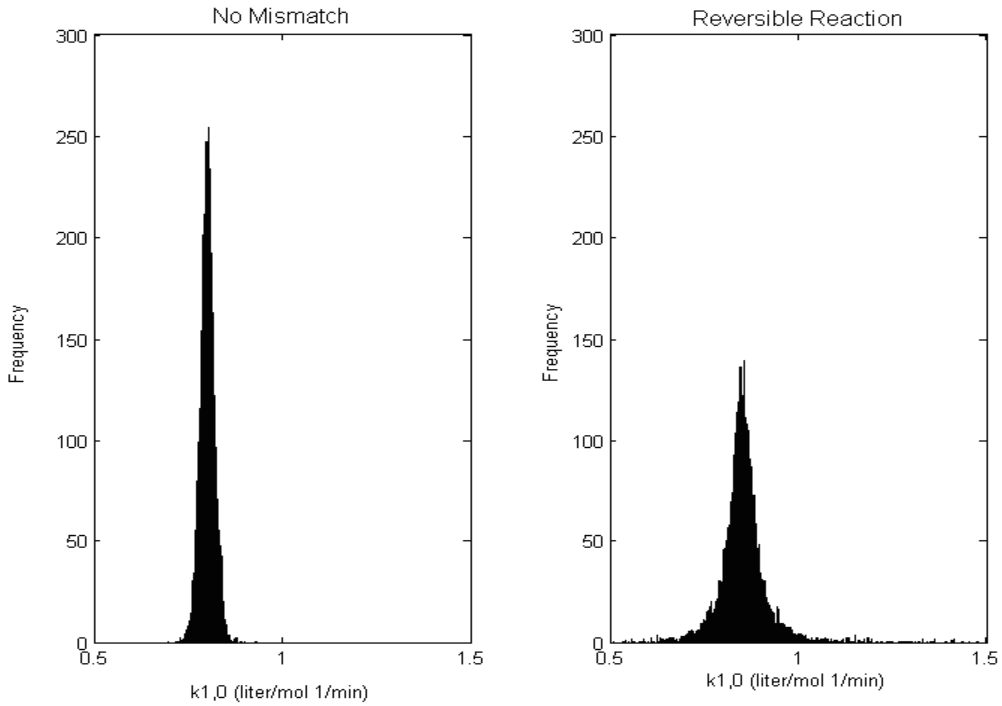

Figure 5.6. The effect of a reversible reaction on the variance of $k_{1,0}$ when a small amount of sensor noise is used.

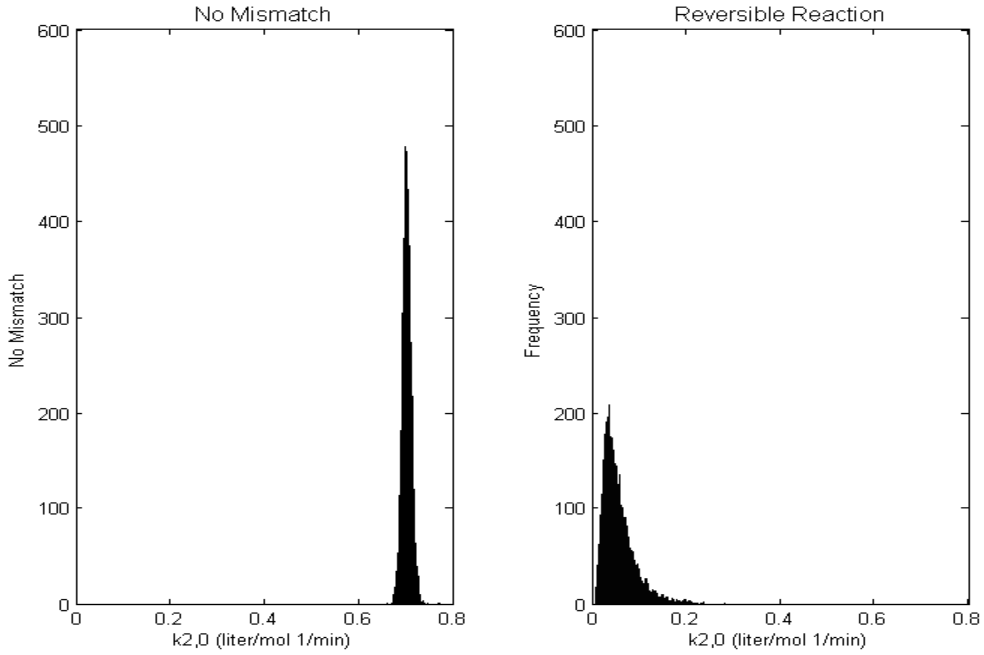

Figure 5.7. The effect of a reversible reaction on the variance of $k_{2,0}$ when a small amount of sensor noise is used.

Model mismatch caused by neglecting the reversible reaction still leads to an increase in the variance of the frequency factors when a large amount of sensor noise is used. This can be seen in Figure 5.8 which shows the effect of a reversible reaction. The results were similar for both $k_{1,0}$ and $k_{2,0}$ for this case. The standard deviations of these results are provided in Tables 5.5 and 5.6.

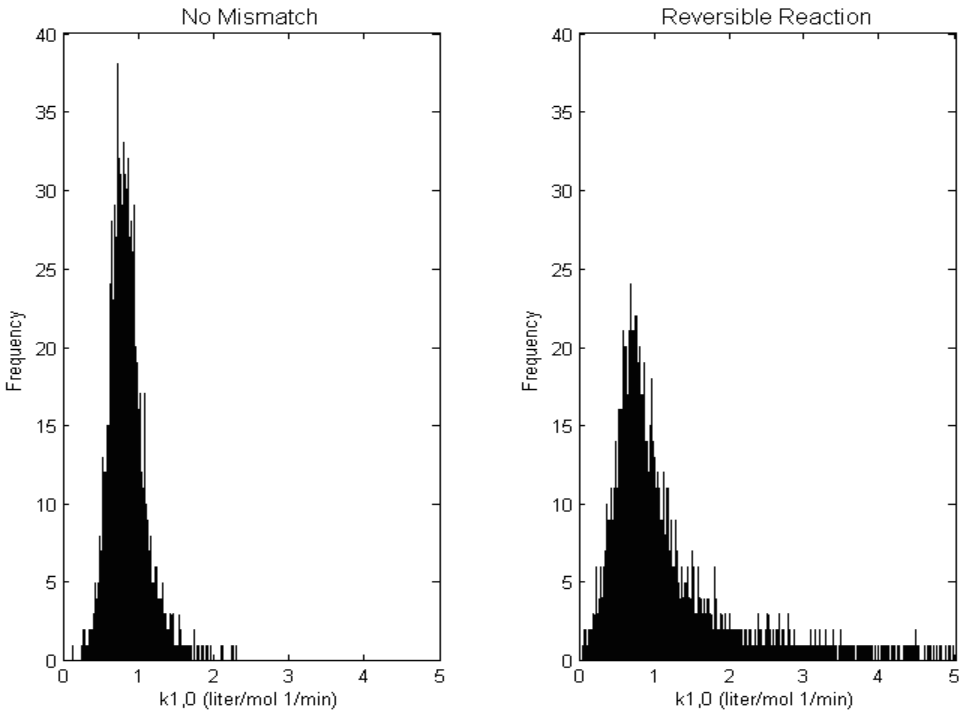

Figure 5.8. The effect of a reversible reaction on the variance of $k_{1,0}$ when a large amount of sensor noise is used.

In the final type of model mismatch the base case rate equation for reaction 1, which is the assumed rate equation in the approximate model, is given as:

$$r = k(T)C_A^{\alpha}C_B^{\beta} \tag{5.11}$$

where α and β are both equal to one. However, in the process model α is now assumed to have a value of 0.75 and β is assumed to have a value of 1.25. It can be seen in Figures 5.9 and 5.10 that this type of model mismatch also results in an increase in the variance of the frequency factors.

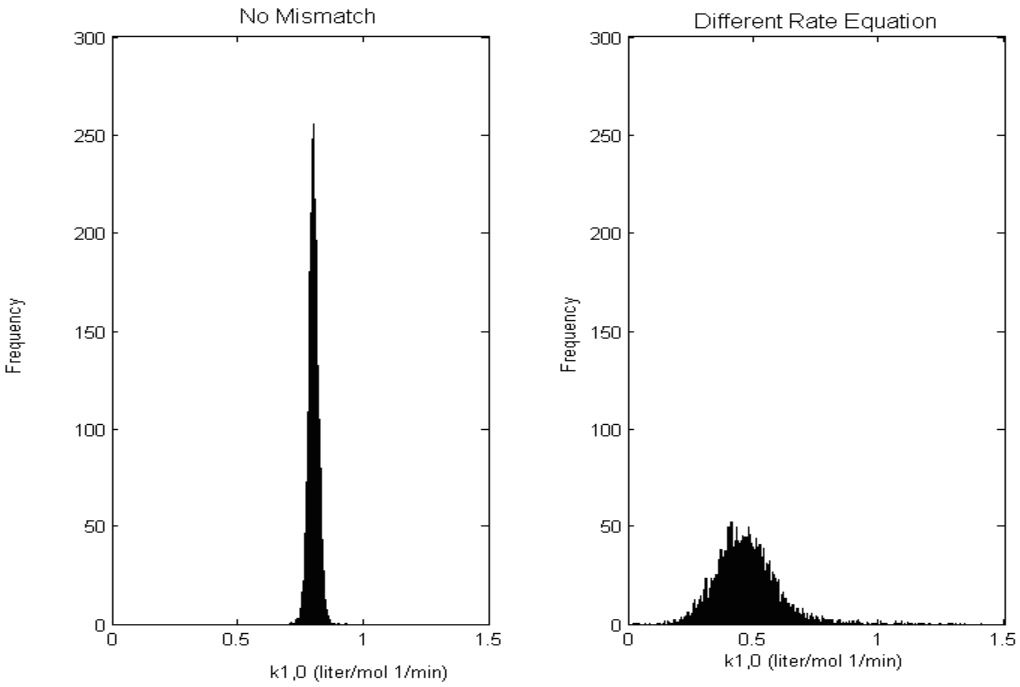

Figure 5.9. The effect of a different rate equation on the variance of $k_{1,0}$ when a small amount of sensor noise is used.

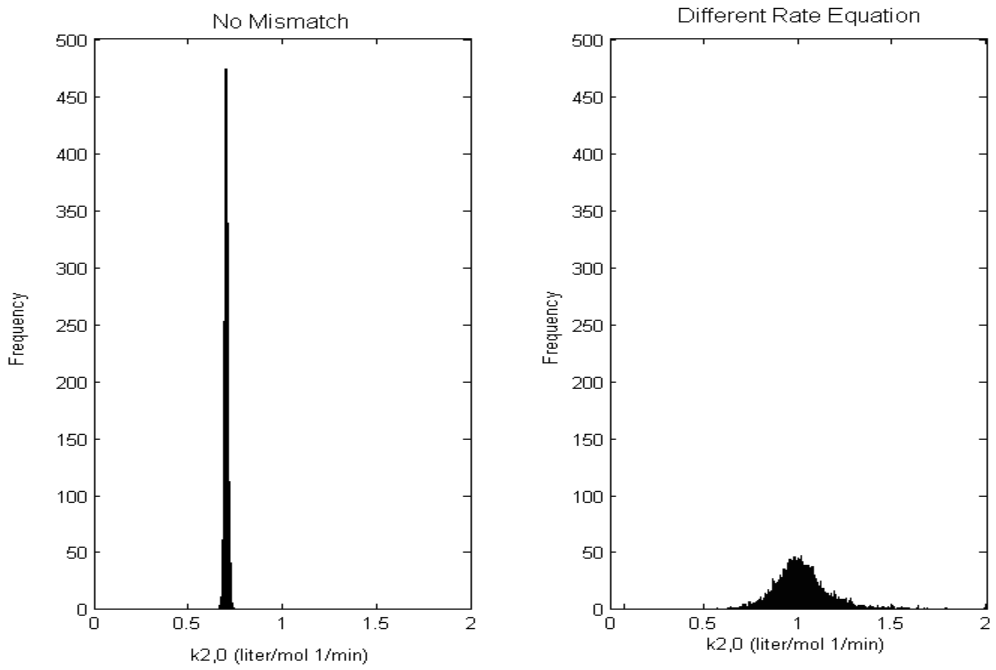

Figure 5.10. The effect of a different rate equation on the variance of $k_{2,0}$ when a small amount of sensor noise is used.

Model mismatch caused by an incorrect rate equation still leads to an increase in the variance of the frequency factors when a large amount of sensor noise is used. This can be seen in Figure 5.11 which shows the effect of an incorrect rate equation. The standard deviations of these results are provided in Tables 5.5 and 5.6. The results were the same for $k_{1,0}$ and $k_{2,0}$ for this case.

Table 5.5: Standard deviation of frequency factors caused by mismatch with a small amount of noise.

Model Parameter	No Mismatch	Reversible Reaction	Different Rate Equation
$k_{1,0}$ (liter/mol·min)	0.02	0.09	1.51
$k_{2,0}$ (liter/mol·min)	0.01	0.03	2.79

Table 5.6: Standard deviation of $k_{1,0}$ (liter/mol·min) with a large amount of noise.

Model Parameter	No Mismatch	Reversible Reaction	Different Rate Equation
$k_{1,0}$ (liter/mol·min)	0.20	1.4	1.55

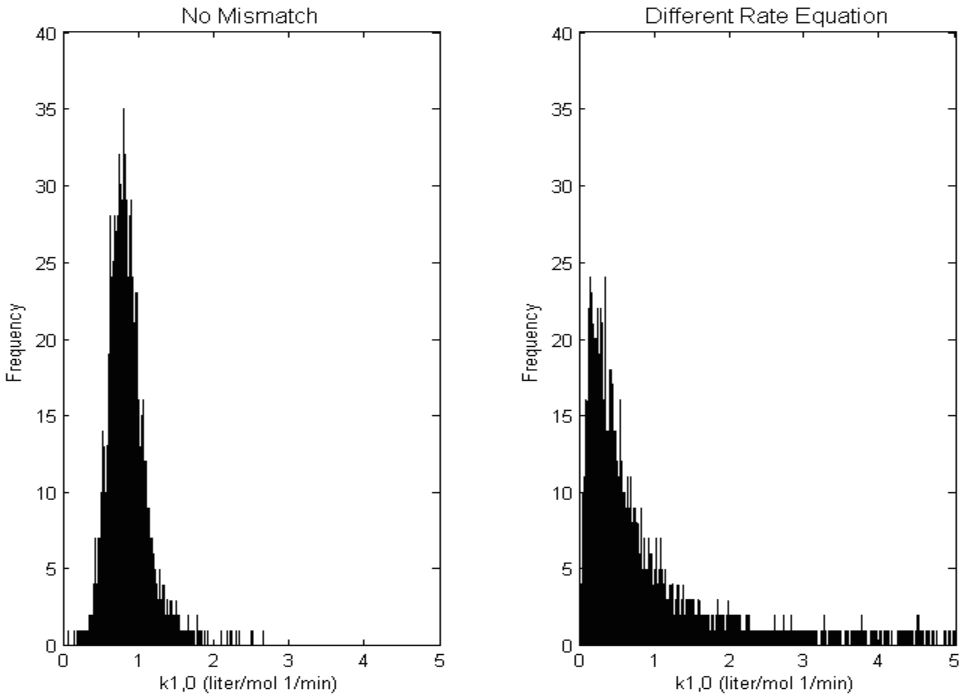

Figure 5.11. The effect of a different rate equation on the variance of $k_{1,0}$ when a large amount of sensor noise is used.

It can be seen from the results provided in this chapter that structural mismatch in the approximate model can be identified by looking at the distribution of the frequency factors for each reaction when a small amount of sensor noise is used. As the structural mismatch in the approximate model is increased, so does the observed variation in the frequency factors. When a large amount of sensor noise is used it is not possible to identify the structural mismatch caused by an error in the activation energies. However, it is still possible to identify the structural mismatch caused by a neglected reversible reaction and an incorrect rate equation when a large amount of sensor noise is used.

CHAPTER 6

DISTILLATION COLUMN STUDY

Separation of chemical species is vital to the chemical process industry. There are many methods that can be used to separate chemical species such as flash distillation, batch distillation, absorption, stripping, and column distillation. Column distillation is the most common method because it can be used in a continuous process and it has a relatively flexible operating window. Distillation columns separate chemical components by taking advantage of the differences in the boiling points of the different species. Chemical plants commonly have from 50 to 90% of their capital invested in separations (Wankat, 1988).

A binary propylene-propane distillation column or C_3 splitter is the unit considered in this chapter. The separation of propylene and propane is very difficult leading to very large distillation columns. A typical C_3 splitter is split into two separate towers because a single tower is usually too tall to be cost effective or safe. They are used in ethylene plants and refineries to produce polymer grade propylene.

6.1 Distillation Column Model

Several assumptions are made in the modeling of the C_3 splitter and they are the same as those used by Hurowitz (1998):

1) Equimolal overflow is assumed.

2) The relative volatility is assumed to be a function of liquid composition and pressure.
3) Pressure is constant throughout the column.
4) All trays have the same Murphree tray efficiency.
5) The column uses a partial reboiler and a total condenser, the reboiler is treated as an ideal stage.

Equilibrium data is represented by a distribution coefficient or K-value which is defined as:

$$K_i = \frac{y_i}{x_i} \tag{6.1}$$

where y_i is the mol fraction of component i in the vapor phase and x_i is the mol fraction of component i in the liquid phase (Wankat, 1988). In general the K-values depend on temperature, pressure, and liquid phase composition (Wankat, 1988). When a system is in equilibrium, fixing any two of the parameters fixes the third.

The relative volatility of a binary mixture is a measure of the ease of separation and a relative volatility of 1 represents an azeotrope or an infinitely difficult separation. The relative volatility of components i and j is defined as:

$$\alpha_{i,j} = \frac{K_i}{K_j}. \tag{6.2}$$

For a binary system:

$$\alpha_{1,2} = \frac{\frac{y_1}{x_1}}{\frac{y_2}{x_2}} = \frac{y_1 x_2}{y_2 x_1} \qquad \text{where} \quad \begin{matrix} y_1 + y_2 = 1 \\ x_1 + x_2 = 1 \end{matrix}. \tag{6.3}$$

This equation for relative volatility of a binary system can then be rearranged into the form:

$$\alpha_{1,2} = \frac{y_1(1-x_1)}{x_1(1-y_1)}. \tag{6.4}$$

When the equilibrium relative volatility and the liquid composition are known the vapor composition can be found by solving for y_1 where:

$$y_1 = \frac{\alpha_{1,2} x_1}{1 + (\alpha_{1,2} - 1)x_1}. \tag{6.5}$$

This equation expresses the vapor phase mol fraction of the more volatile component, y_1, as a function of the liquid phase mol fraction of the more volatile component, x_1, and the relative volatility of the system, $\alpha_{1,2}$ (Hurowitz, 1998).

The relative volatility of the propylene-propane system is modeled with a quadratic equation developed by Finco (1987). The relative volatility is a function of pressure and mol fraction of propylene in the liquid phase. The equation is given as:

$$\begin{aligned} \alpha &= a_0 - a_1 x - a_2 x^2 \\ a_0 &= 1.285500 - 0.00044600P \\ a_1 &= 0.088008 - 0.00010350P \\ a_2 &= 0.052215 - 0.00014607P \end{aligned} \tag{6.6}$$

where P is pressure in psia and x is the mol fraction of propylene in the liquid phase. The separation of propylene and propane is known to be very difficult and this can be shown by determining the range of the relative volatility. At 211 psia the relative volatility of this system is between 1.1 and 1.2 indicating a very difficult separation.

The distillation column design parameters are similar to those used by Hurowitz (1998) and are listed in Table 6.1. The operating conditions of the column are found by doing stage-to-stage calculations. The feed flow rate, feed composition, distillate composition, and bottoms composition are all specified. The distillate flow rate and bottoms flow rate are found by doing an overall column balance. The material balance equations are:

$$D = \frac{F(z - x_B)}{x_D - x_B} \tag{6.7}$$

$$B = F - D \tag{6.8}$$

where D is the distillate flow rate, F is the feed flow rate, z is the mol fraction of propylene in the feed, x_B is the mol fraction of propylene in the bottoms product, x_D is the mol fraction of propylene in the distillate product, and B is the bottoms flow rate.

The secant-method is used to solve for the reflux ratio that yields the desired product compositions based on the given flow rates of each stream. An initial reflux ratio is estimated by using the Fenske-Underwood-Gilliland procedure. The reboiler is treated as an ideal stage so the bottoms product composition is the same as the liquid composition in the reboiler. The vapor composition in the reboiler can be found by using equation (6.5). Vapor and liquid compositions at each tray are calculated by using the

compositions at the tray below it. The following equations are used to calculate tray compositions:

$$y_i = y_{i-1} + EM\left[\frac{\alpha_{1,2}x_i}{1+x_i(\alpha_{1,2}-1)} - y_{i-1}\right] \tag{6.9}$$

$$x_{i+1} = \frac{Lx_i + V(y_i - y_{i-1})}{L} \tag{6.10}$$

where EM is the Murphree tray efficiency, L is the liquid flow rate in the column, V is the vapor flow rate in the column, and i is the tray number. Above the feed tray L is equal to the reflux and V is equal to the reflux plus the distillate flow rate. Below the feed tray L is equal to the reflux plus the feed flow rate and V is equal to the reflux plus the distillate flow rate.

Table 6.1: C_3 Splitter Design Parameters

Total Number of Trays	232
Feed Tray Location (from bottom)	64
Column Pressure	211
Murphree Tray Efficiency	0.75
Reflux Condition	Saturated Liquid
Feed Condition	Saturated Liquid

6.2 Model Mismatch

The type of model mismatch considered here for a distillation column is a difference in the relative volatility used by the process and approximate models. Equation (6.6) is modified so that the relative volatility calculated in the approximate

model is different from the value used in the process model. The equation used by the approximate model is as follows:

$$\begin{aligned} \alpha &= a_0 - a_1 x - a_2 x^2 \\ a_0 &= 1.285500 - 0.00044000P \\ a_1 &= 0.088008 - 0.00010360P \\ a_2 &= 0.052220 - 0.00014609P \end{aligned} \quad . \tag{6.11}$$

Larger errors in the relative volatility equation were attempted, but the calculations in the approximate distillation column model would not converge. Although the error is not very large, the effect is still obvious. The process model uses equation (6.6) to calculate the relative volatility.

6.3 Results

There are five process measurements used to parameterize the approximate distillation column model, two flow measurements, two composition measurements, and one pressure measurement. The flow meter is assumed to be an orifice flow meter for large amounts of noise and a magnetic flow meter for small amounts of noise. The composition analyzer is assumed to have a repeatability of ±1% for small amounts of noise and ±10% for large amounts of noise. The repeatability of the pressure sensor is assumed to be ±0.1% (Riggs, 2001) for all trials. The variation in the tray efficiency was generated using 5,000 simulations.

When looking only at the effect of sensor noise on the variation of the calculated tray efficiency, it can be seen in Figure 6.1 that reducing the amount of noise greatly

reduces the variation in the tray efficiency. The standard deviations of these results are provided in Table 6.2.

Table 6.2: Standard deviation of tray efficiency caused by sensor noise.

Model Parameter	Small Amount of Noise	Large Amount of Noise
Tray Efficiency	1.3×10^{3}	1.1×10^{2}

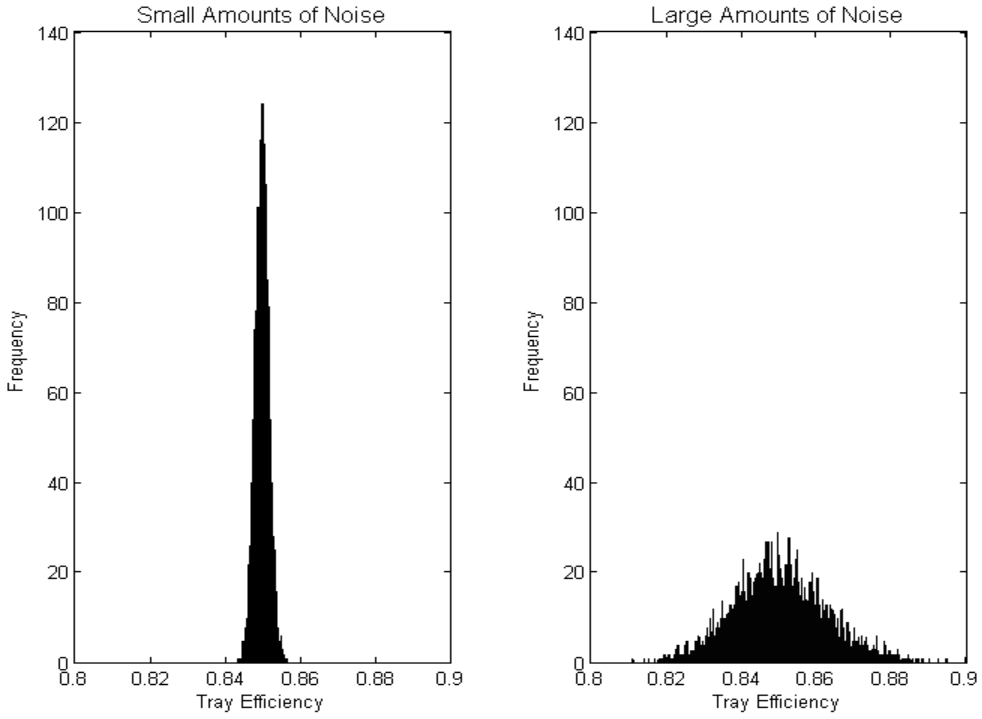

Figure 6.1. The effect of sensor noise on the variance of the tray efficiency.

Adding structural model mismatch also significantly increases the variance of the calculated tray efficiency as seen in Figure 6.2. When there is no model mismatch between the process model and the approximate model the variation in the calculated tray efficiency is that caused by sensor noise. Structural mismatch in the form of an error in the calculation of the relative volatility leads to an increase in the variation of the calculated tray efficiency.

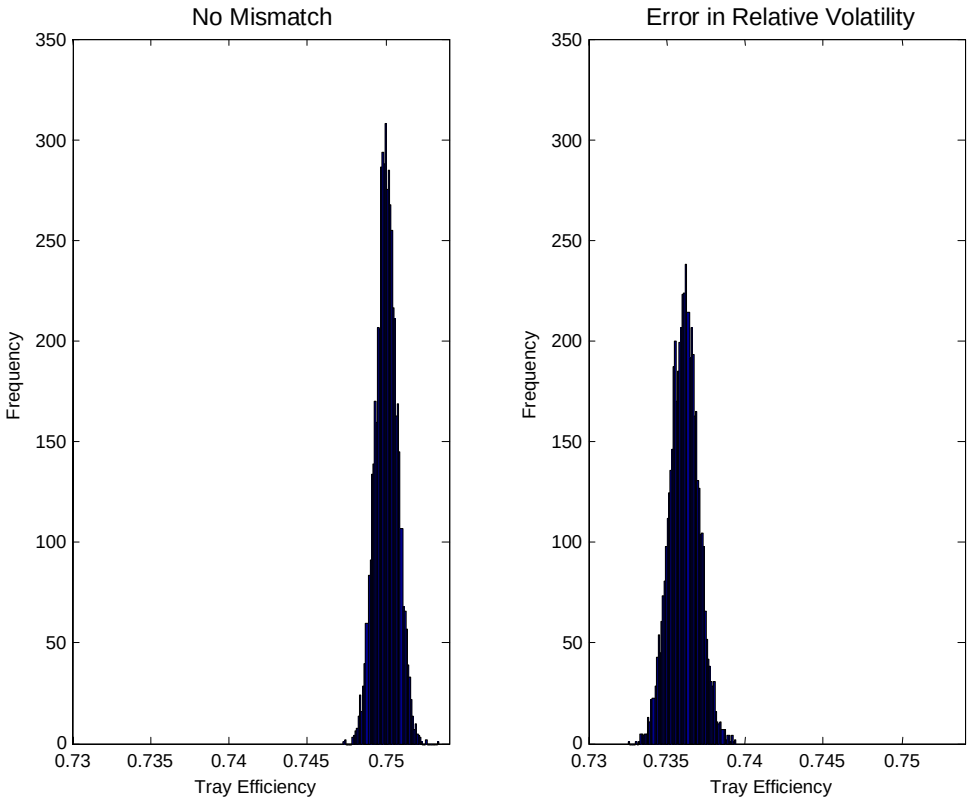

Figure 6.2. The effect of an error in the relative volatility on the variance of the tray efficiency.

When a large amount of sensor noise is used, there is not a significant increase in the variation of the calculated tray efficiency when structural model mismatch is incorporated. The variance is not increased because the variation caused by the magnitude of the sensor noise outweighs the variation caused by the structural model mismatch. The standard deviations of these results are provided in Table 6.3.

Table 6.3: Standard deviation of tray efficiency caused by mismatch with a small amount of noise.

Noise	No Mismatch	Error in Relative Volatility
Small Amount	1.3×10^{3}	1.9×10^{3}
Large Amount	1.1×10^{2}	1.0×10^{2}

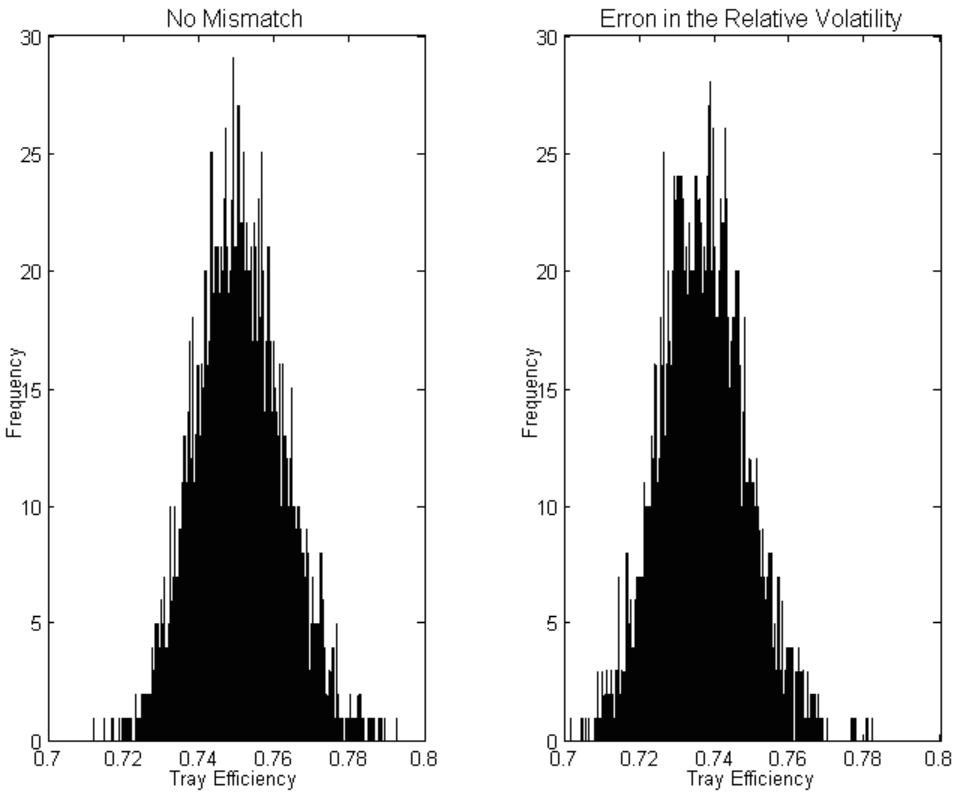

Figure 6.3. The effect of an error in the relative volatility on the variance of the tray efficiency when a large amount of noise is used.

It can be seen from the results provided in this chapter that for this particular case structural mismatch in the approximate model can be identified by looking at the distribution of the calculated tray efficiency when a small amount of noise is used. However, when a large amount of noise is used, it is not possible to identify structural mismatch caused by the error in the calculation of the relative volatility in the approximate model due to the magnitude of sensor noise.

CHAPTER 7

FURNACE STUDY

An ethylene furnace is the most complex model considered in this study. Ethylene is a critical building block for many commercial products because of its highly reactive double bond. Ethylene is used in the production of plastics, textiles, paper, solvents, dyes, food additives, pesticides, and pharmaceuticals (Yan, 2000).

With today's technology a variety of feedstocks can be used to produce ethylene. The feedstock is mixed with dilution steam in order to reduce the partial pressure and slow coke formation (Yan, 2000). The mixture then enters the furnace and is pyrolysised by heat into smaller species such as ethylene. For this study the feedstock is assumed to be an ethane/propane mixture that is commonly used in industry.

7.1 Complex Furnace Model

The furnace model used in this study is basically the same as that used by Yan (2000) with a few modifications. The model developed by Yan was used to study the plant-wide time-domain optimization of an ethylene plant and included the formation of coke on the reactor tube walls. The study conducted here does not require the use of a coke formation model and this part of the model was neglected and an assumed coke thickness was used. Yan also made the assumption of a constant heat flux throughout the reactor and this assumption was assumed to be incorrect for this study. Instead, the assumption of a constant outer tube wall surface temperature was made and the reactor

outlets for the model used in this study and the model used by Yan are nearly identical under the same operating conditions.

7.1.1 Reaction Scheme

The ethylene furnace model is assumed to have an ethane/propane feed and the reaction scheme used is that proposed by Froment and Sundaram (1978). The reaction scheme uses a free radical mechanism that includes three consecutive stages: initiation, propagation, and termination (Froment, 1978).

Initially, the species in the reactor are quickly heated to a high temperature breaking chemical bonds. When these bonds are broken, free radicals are produced which are highly reactive molecules that have an unpaired electron. This step is referred to as the initiation stage and an example is as follows:

$$A \rightarrow B\bullet + C\bullet$$

where A is the reactant and $B\bullet$ and $C\bullet$ are the free radicals or intermediates.

The free radicals produced in the initiation stage can then react with other stable species to produce additional intermediates. This step is referred to as the propagation stage and an example is as follows:

$$D + C\bullet \rightarrow E + F\bullet$$

where $F\bullet$ is a new intermediate.

The free radicals can then react with each other to produce a final stable product. This step is referred to as the termination stage and an example is as follows:

$$G\bullet + H\bullet \rightarrow I\,.$$

It is assumed that the reactions are elementary and therefore the order corresponds to the molecularity (Froment, 1978). This assumption leads to the elementary reaction rate for each reaction so that for a given reaction:

$$aA + bB \rightarrow cC + dD$$

the reaction rate is given as:

$$r = k(T)C_A^a C_B^b \tag{7.1}$$

where r is the reaction rate, $k(T)$ is the rate constant, C_A is the concentration of reactant A, and C_B is the concentration of reactant B. The rate constant is assumed to have Arrhenius temperature dependence and is given as:

$$k(T) = k_0 \exp\left(-\frac{E_a}{RT}\right) \tag{7.2}$$

where k_0 is the frequency factor, E_a is the activation energy, R is the gas constant, and T is the temperature.

The complex reaction network proposed by Froment (1978) is given in Appendix A. There are eleven species that are assumed to be present in the reactor for an E/P feed and they are:

$$H_2,\ CH_4,\ C_2H_2,\ C_2H_4,\ C_2H_6,\ C_3H_6,\ C_3H_8,\ C_4H_6,\ 1-C_4H_8, n-C_4H_{10},\ C_5^+$$

where C_5^+ is a lumped product of all species larger than or equal to C_5H_{10}. There are also eleven free radical species that are assumed to be present in the reactor and they are:

$$H\bullet,\ CH_3\bullet,\ C_2H_3\bullet,\ C_2H_5\bullet,\ C_3H_5\bullet,\ 1-C_3H_7\bullet,\ 2-C_3H_7\bullet,\ C_4H_7\bullet,$$

$$1-C_4H_9\bullet,\ 2-C_4H_9\bullet,\ C_5H_{11}\bullet.$$

7.1.2 Reactor Model

The PFR model is used in this study to model the ethylene furnace. The PFR model is based on two underlying assumptions and they are:

1) There is no axial mixing or axial heat transfer.
2) Residence time for all fluid elements through the reactor, from the inlet to outlet, are of equal duration.

The residence time is determined by dividing the reactor volume by the volumetric feed rate at the average reactor temperature and pressure.

The reactor model equations are given by Yan (2000) as:

$$\frac{dF_i}{dZ} = -\frac{\pi \cdot d_t^2}{4} \cdot \sum_j s_{i,j} \cdot r_i \tag{7.3}$$

$$\frac{dT}{dZ} = \frac{1}{\sum F_j C_{P_j}} \left[Q(Z)\pi \cdot d_t + \frac{\pi \cdot d_t^2}{4} \sum_i r_i (-\Delta H)_i \right] \tag{7.4}$$

where F_i is the molar flow rate of species i, d_t is the inner tube diameter, $s_{i,j}$ is the stoichiometric coefficient of species j in reaction i, Z is the axial reactor coordinate, C_{P_j} is the heat capacity of species j, $Q(Z)$ is the heat flux, T is temperature, and ΔH_i is the heat of reaction i.

The pressure drop in the furnace tubes is addressed by using a momentum balance (Bennett, 1974). The momentum balance is given as:

$$\frac{dP}{dL} = -G \cdot \frac{du}{dL} - 2 \cdot \frac{f_r}{\rho \cdot D \cdot g_c} \cdot G^2 \tag{7.5}$$

where P is pressure, L is length, G is mass velocity, u is the average velocity of the gas, f_r is the pressure drop factor, ρ is the gas density, D is the inner tube diameter, and g_c is the gravity constant. Simplifications are made in order to rearrange this equation. First, the whole tube is divided into twenty sections while the mass velocity, G, is assumed to be constant for each section (Yan, 2000). Second, for each section, since the inlet and outlet temperature do not vary significantly, the isothermal state equation:

$$\rho = \rho_0 \cdot \frac{P}{P_0} \tag{7.6}$$

is assumed to be applicable (Yan, 2000). These simplifications allow for equation (7.5) to be rearranged into the following form:

$$\rho \cdot \frac{dP}{dL} - G^2 \cdot \frac{dP}{P \cdot dL} + 2 \cdot f_r \cdot \frac{G^2}{D \cdot g_c} = 0 . \tag{7.7}$$

Further simplification yields the final differential equation used for the pressure drop and the equation is as follows:

$$\frac{dP}{dZ} = -\frac{2 \cdot f_r \cdot \left(\frac{G^2}{D \cdot g_c} \right)}{\rho - \frac{G^2}{P}} \tag{7.8}$$

where Z is equal to L.

The resulting set of Ordinary Differential Equations (ODEs) are found to be highly coupled and stiff because the reactions involving the free radicals are much faster than those involving the stable molecular species. The Livermore Solver for Ordinary

Differential Equations (LSODE) integration package is used to integrate each of the ODEs through the length of the reactor. LSODE is very effective for this application because it is a "variable order/variable step size" method (Riggs, 1994).

7.2 Simplified Furnace Model

A simplified furnace model is developed to determine the effect of structural model mismatch on the variation of the model parameters. The simplified model is the same as the complex model except there are fewer reactions and the free radical species are neglected. The simplified model also neglects species that are present in very small amounts such as $1-C_4H_8$ and $n-C_4H_{10}$.

The first step in developing the simplified furnace model was to come up with a suitable reaction scheme that accounts for all the assumed species present in the reactor. This was accomplished by integrating in small steps at the reactor inlet of the complex model and determining the concentration of each species after each step. This allowed for the determination of which species are being consumed and which are being formed and also at what rate. This procedure along with the use of element balances yielded an initial set of assumed reactions.

The next step was to determine the kinetics of each reaction and this was accomplished by using the rate of formation and concentration of each species at the end of each tube section in the complex model. As mentioned earlier, the reactor tubes are separated into twenty sections. The complex model was modified so that the temperature of the fluid in the reactor stayed constant allowing for the calculation of the kinetic

parameters of the assumed reaction scheme. The reaction rate of each of the reactions is assumed to be in the form of:

$$r = k_0 \exp\left(-\frac{E_a}{RT}\right) C_A^{\alpha} \tag{7.9}$$

where r is the rate of the reaction, k_0 is the frequency factor, E_a is the activation energy, R is the gas constant, T is the temperature, C_A is the concentration of reactant A, and α is the order with respect to reactant A. Using the data generated with the complex model, r, R, T, and C_A are all known. The other parameters, k_0, E_a, and α are found using the Solver function in Excel so that the error between the calculated rate of formation and the actual rate of formation of each species is minimized.

The resulting simplified model consists of eight total reactions which can be seen in Appendix A. The prediction of each species concentration as well as the temperature and pressure were compared at the end of each tube section for both models to determine how well they correlate. It was found that the predictions of both models correlate somewhat well at the assumed operating conditions and these results can be seen in Appendix B.

7.3 Results

The process measurements used to parameterize the approximate model are two temperature measurements, two flow measurements, two pressure measurements, and a composition analyzer on the reactor inlet and effluent. A small amount of sensor noise corresponds to the use of magnetic flow meters, RTDs, and ±1% repeatability for the

composition analyzers. A large amount of sensor noise corresponds to the use of orifice flow meters, thermocouples, and ±20% repeatability for the composition analyzers. The pressure sensors are assumed to have a repeatability of ±0.1% for all trials. The variation in the reactor tube temperature was generated using 25,000 simulations.

When looking only at the effect of sensor noise on the variation of the calculated tube temperature, it can be seen in Figure 7.1 that reducing the amount of sensor noise greatly reduces the variance in the tube temperature. The standard deviations of these results are provided in Table 7.1.

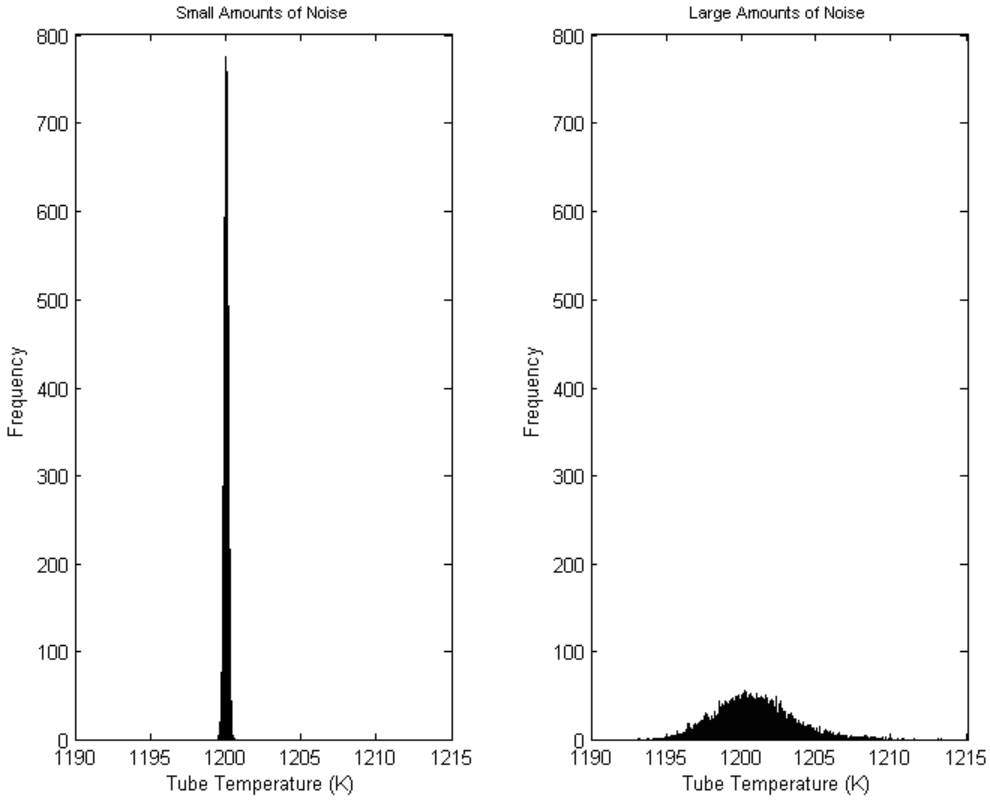

Figure 7.1. The effect of sensor noise on the variance of the tube temperature.

Table 7.1: Standard deviation of tube temperature (K) caused by sensor noise.

Model Parameter	Small Amount of Noise	Large Amount of Noise
Tube Temperature	0.14	2.67

Adding structural model mismatch between the approximate model and the process model also significantly increases the variance of the calculated tube temperature as can be seen in Figure 7.2. When there is no mismatch the variation is that caused by sensor noise. Structural mismatch in the form of the approximate model being simplified leads to an increase in the variance of the tube temperature. When a large amount of sensor noise is used it is still possible to identify the structural model mismatch as can be seen in Figure 7.3. The standard deviations of these results are provided in Table 7.2.

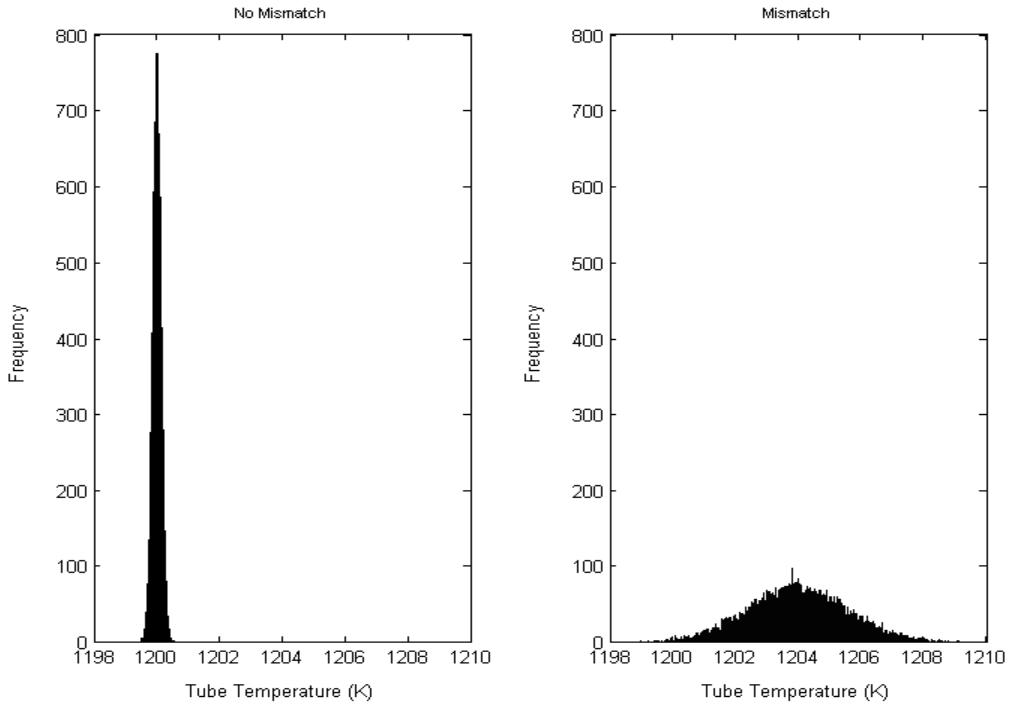

Figure 7.2. The effect of model mismatch on the variation of the tube temperature when a small amount of sensor noise is used.

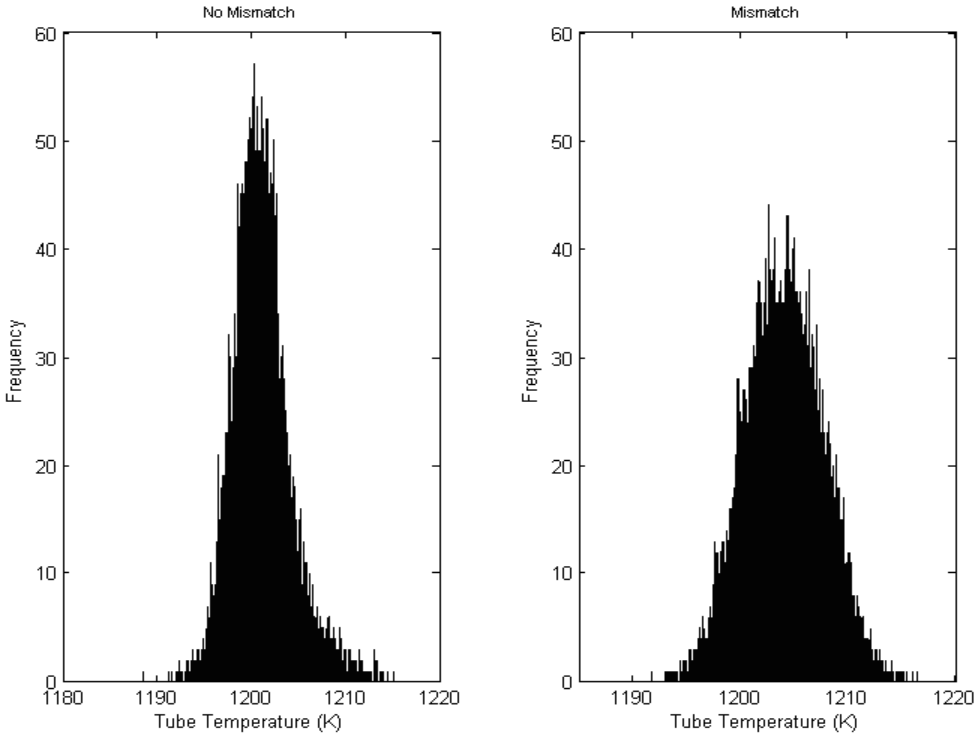

Figure 7.3. The effect of model mismatch on the variation of the tube temperature when a large amount of sensor noise is used.

Table 7.2: Standard deviation of tube temperature (K) caused by mismatch.

Noise	No Mismatch	Simplified Model
Small Amount	0.14	1.56
Large Amount	2.67	3.29

CHAPTER 8

VALUE OF IMPROVED SENSOR READINGS

Sensor noise is inherent to all sensors used on chemical processes. It has been shown in the previous chapters that increased sensor noise leads to an increase in the variation of the calculated model parameters. It is theorized that decreasing the amount of variation in the model parameters will increase the performance of an RTO application leading to the question of whether the cost of a new sensor will lead to a justifiable increase in profit attained by the optimization application.

Data reconciliation is used throughout the chemical process industry to reject excessively noisy process measurements. However, the distribution of the noise associated with a sensor may be within the acceptable limits of the data reconciliation algorithm but a better sensor should decrease the noise distribution resulting in a decrease in the variation of a calculated model parameter.

Large amounts of sensor noise can cause an RTO application to move towards a new optimum even though the optimum has not changed since the last RTO execution. The amount of profit lost due to unnecessary RTO moves depends on the shape of the optimization curve. The ethylene furnace is used to study how increased amounts of sensor noise affect the overall profit attained for different shapes of the optimization curve.

8.1 CSTR

The problem studied here to determine how sensor noise effects the true profit attained when optimizing the operating temperature of a CSTR is taken from Riggs et al. (2001). A series reaction is assumed to take place in the reactor and is given as:

$$A \rightarrow B \rightarrow C\,. \tag{8.1}$$

The rate equation for each of the reactions is assumed to be in the form of:

$$r = kC\exp\left(\frac{-E}{RT}\right) \tag{8.2}$$

where r is the rate of reaction, k is the frequency factor, C is the concentration of the reactant, E is the activation energy, R is the gas constant, and T is the temperature in the reactor.

An objective function is developed that accounts for the cost of the feed as well as the value of the products. Two levels of sensor noise are considered in this study and the total true profit attained is compared for each case. A small amount of sensor noise corresponds to the use of an RTD, a magnetic flow meter, and ±1% for the composition analyzer. A large amount of sensor noise corresponds to the use of a thermocouple, an orifice flow meter, and ±20% for the composition analyzer.

A graph of the profit versus the reactor operating temperature also called the optimization curve is shown in Figure 8.1. The graph shows that the true optimum operating temperature is approximately 296 K at a profit of approximately $1.52 per second. It can be seen in Figure 8.2 that when a large amount of sensor noise is used the variation in the true profit attained is less than $0.003 per second. When a small amount

of sensor noise is used the variation in the true profit attained is decreased. All values of the true profit attained are summed for each case revealing that when the small amounts of noise are used there is an increase in the overall profit of approximately 0.2% which amounts to $95,600 per year for this particular case. The results in Figure 8.2 were generated using 100,000 simulations.

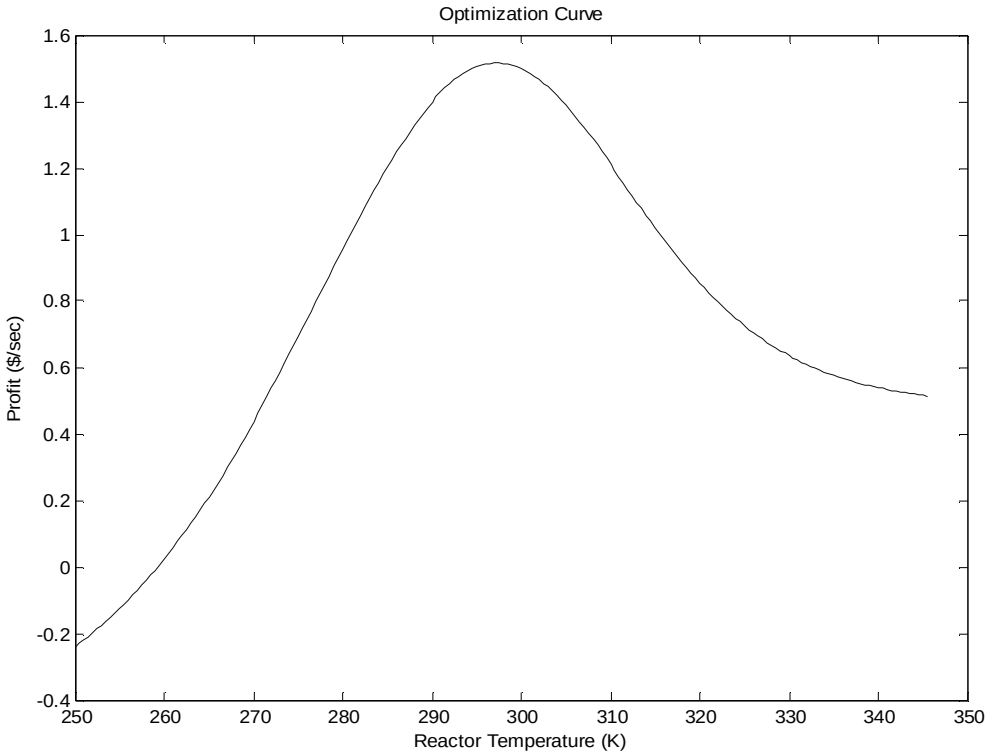

Figure 8.1. CSTR optimization curve.

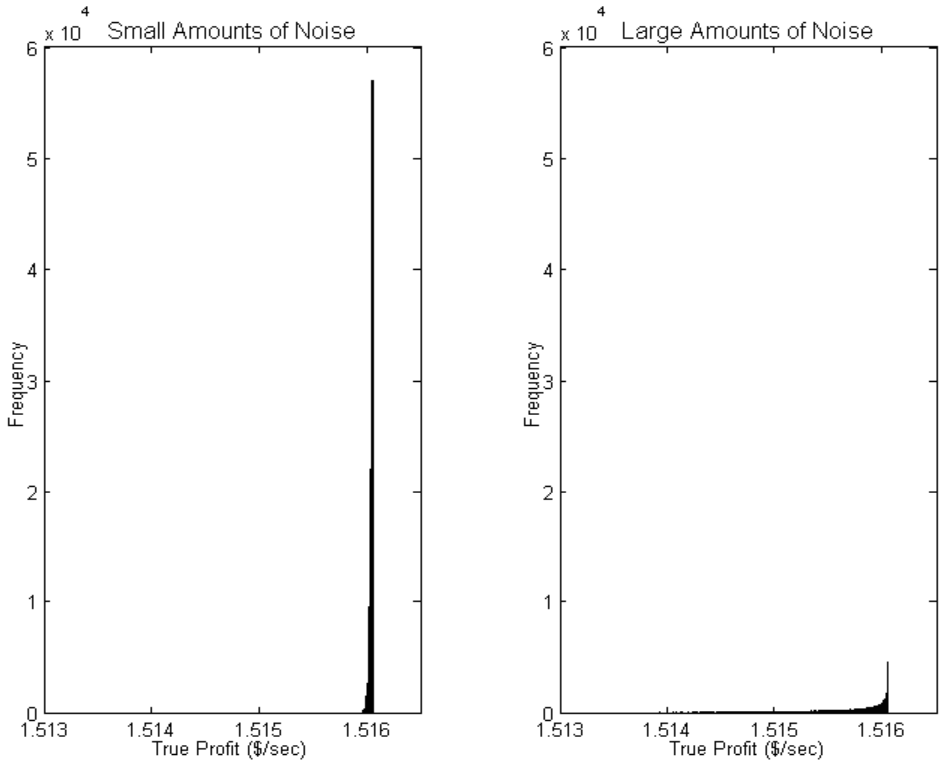

Figure 8.2. The effect of sensor noise on the variation of true profit.

8.2 Distillation Column

The C_3 splitter model from Chapter 6 is modified and used here to determine how sensor noise effects the true profit attained when optimizing a distillation column. The model is modified to account for the energy consumption associated with the reboiler and condenser so that the objective function accounts for the cost of the feed, values of the products, and utility usage.

The case studied here is a one dimensional optimization study where the optimization variable is the amount of propylene in the bottoms product. A small amount of sensor noise corresponds to the use of orifice flow meters and ±10% on the

composition analyzers. A large amount of sensor noise corresponds to the use of orifice flow meters and ±30% on the composition analyzers. The repeatability of the pressure sensor is assumed to be ±0.1% for both cases.

The distillation column optimization curve can be seen in Figure 8.3. The plot shows that the true optimum bottoms propylene mol fraction is approximately 0.018 at a profit of approximately $6.214 per second. It can be seen in Figure 8.4 that when a large amount of sensor noise is used the variation in the true profit attained is less than $0.003 per second. When a small amount of sensor noise is used the variation in the true profit is decreased. All values of the true profit attained are summed for each case revealing that when a small amount of noise is used there is an increase in overall profit of approximately 0.004% which amounts to $7,800 per year for this particular case. The results in Figure 8.4 were generated using 50,000 simulations.

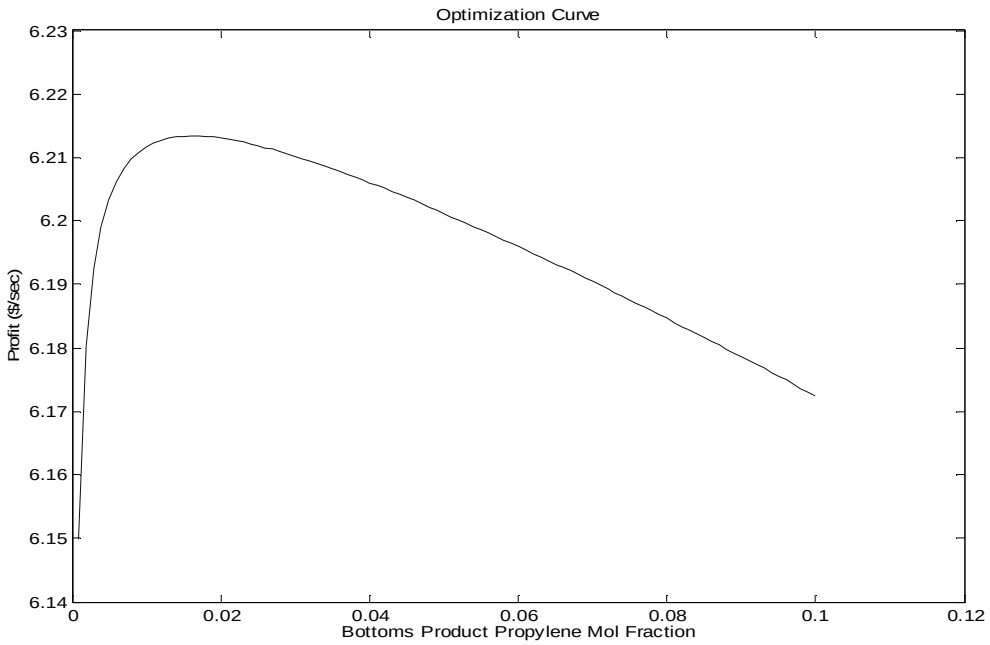

Figure 8.3. Distillation column optimization curve.

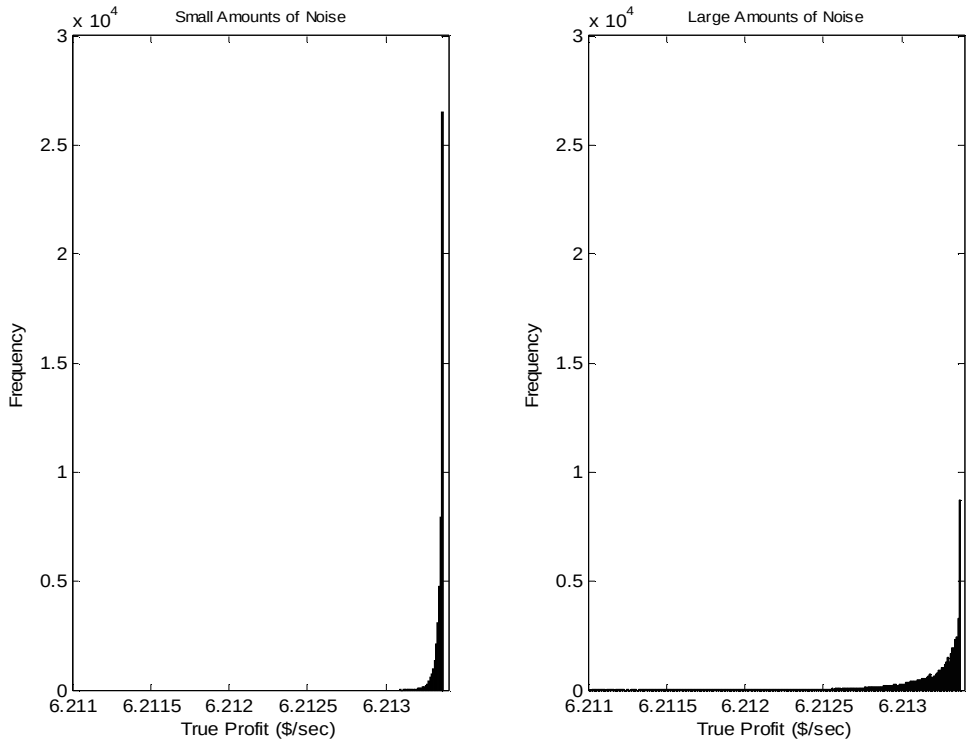

Figure 8.4. The effect of sensor noise on the variation of true profit.

8.3 Furnace

The complex ethylene furnace model from Chapter 7 is modified and used here to determine how sensor noise effects the true profit attained when optimization is applied. The objective function developed for this unit accounts for the cost of the feed, the value of the products, and the cost of the dilution steam. Fuel costs and the value of the hydrogen and methane are neglected in the objective function because the hydrogen and methane produced in the furnace is assumed to be recycled as fuel to the furnace as is the case for most industrial applications (Yan, 2000).

The case studied here is a one dimensional optimization study where the optimization variable is the dilution steam to hydrocarbon ratio. Previous studies have

shown that the maximum profit in an ethylene furnace is attained at the constraints of maximum feed rate and maximum operating temperature (Yan, 2000), therefore, two assumptions are made here:

1. The furnace is already operating at the maximum allowable feed rate.
2. The furnace is already operating at the maximum allowable temperature.

The true profit attained is compared for two different levels of sensor noise, ±1% and ±20% repeatability, on the composition analyzers. Orifice flow meters, RTDs, and ±1% repeatability on the pressure sensors is used for all trials.

8.3.1 Furnace Results

The optimization curve when the outer tube surface temperature is assumed to be 1200 K is shown in Figure 8.5. It can be seen from this plot that the true optimum is located at a dilution steam to hydrocarbon ratio of approximately 0.6 and a profit of approximately $118,540 per day. Figure 8.6 shows that when a repeatability of ±20% is assumed for the composition analyzers the variation in the true profit attained is less than $200 per day. Reducing the amount of sensor noise to ±1% repeatability on the composition analyzers reduces the variation in the true profit attained to less than $100 per day. The sum of all values for the true profit is compared for each case showing that the smaller amount of sensor noise results in a 0.01% increase in profit which amounts to $4,300 per year for this particular case.

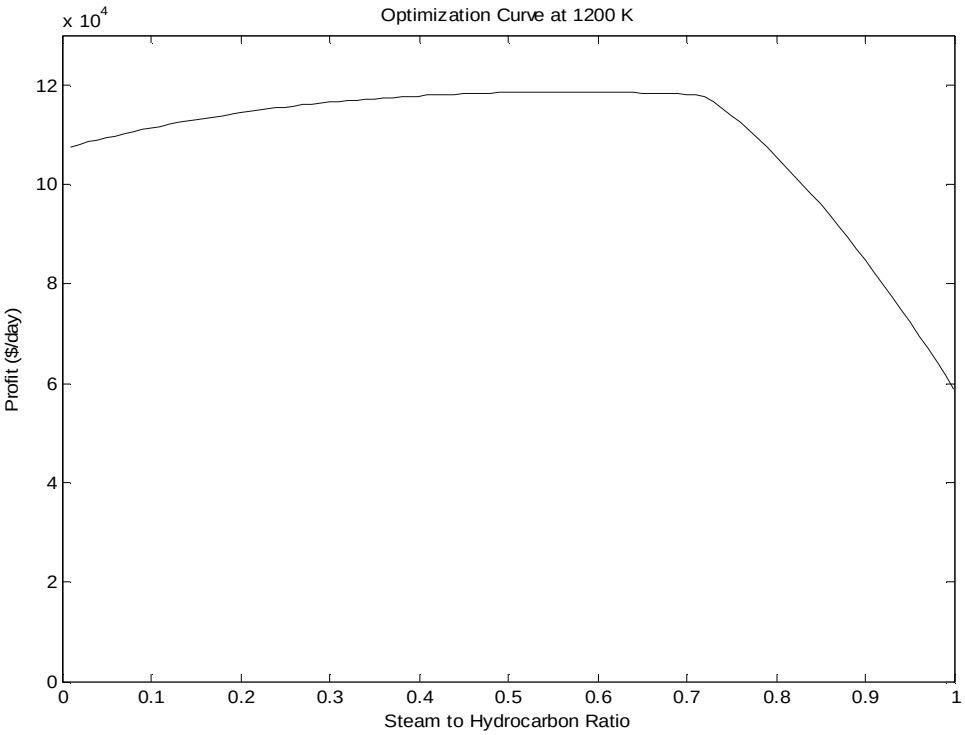

Figure 8.5. Furnace optimization curve for a tube temperature of 1200 K.

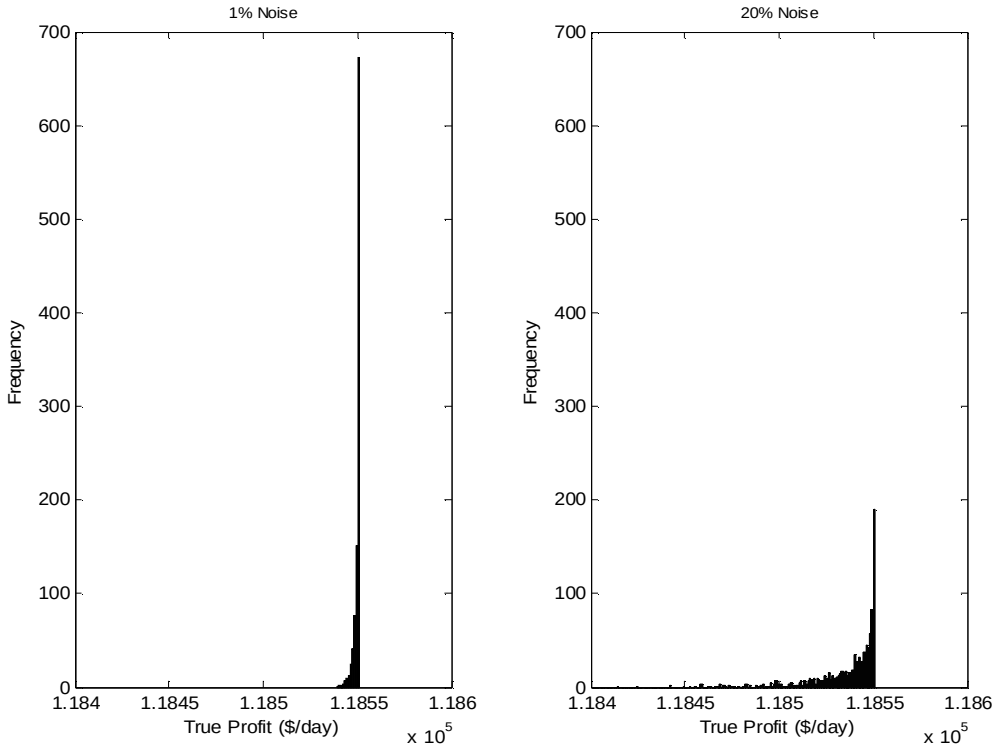

Figure 8.6. The effect of sensor noise on the variation of true profit for a tube temperature of 1200 K.

An outer tube surface temperature of 1415 K is also considered in this study and the optimization curve can be seen in Figure 8.7. The plot shows that the true optimum is located at a dilution steam to hydrocarbon ratio of approximately 0.82 and a profit of approximately $141,000 per day. Figure 8.8 shows that when a repeatability of ±20% is assumed for the composition analyzers the variation in the true profit attained is less than $22,000 per day. When the amount of sensor noise is reduced to ±1% repeatability on the composition analyzers, the reduction in the variation of the true profit attained is barely noticeable. The sum of all values for the true profit is compared for each case

showing that the smaller amount of sensor noise results in a 0.3% increase in profit which amounts to $155,500 per year for this particular case.

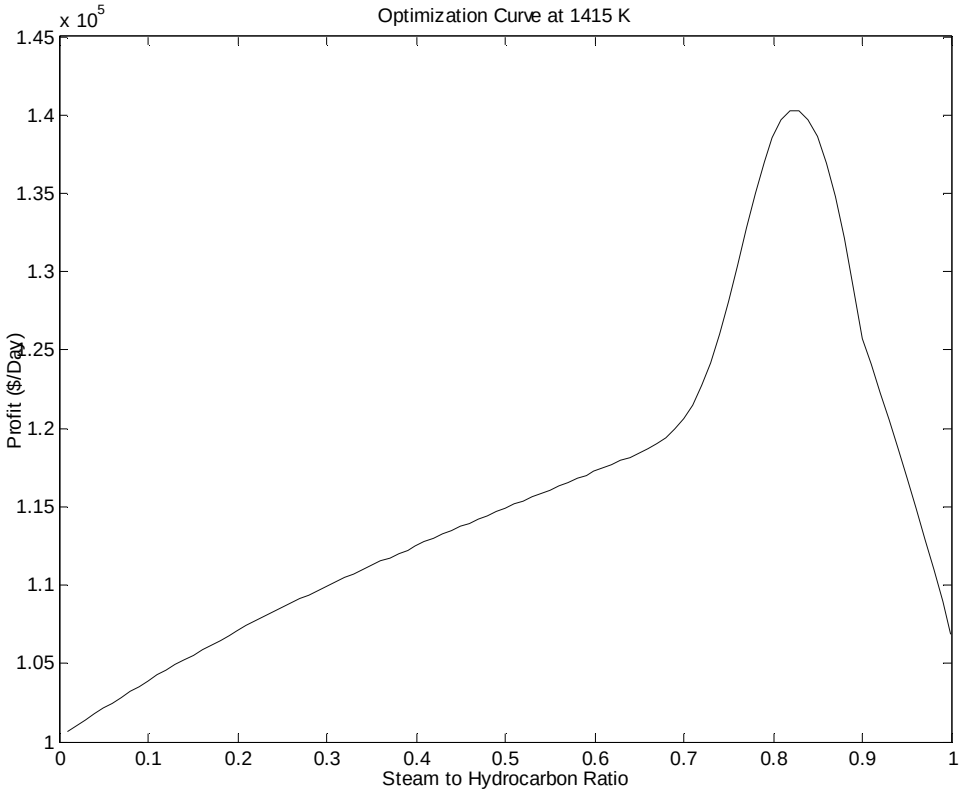

Figure 8.7. Furnace optimization curve at 1415 K.

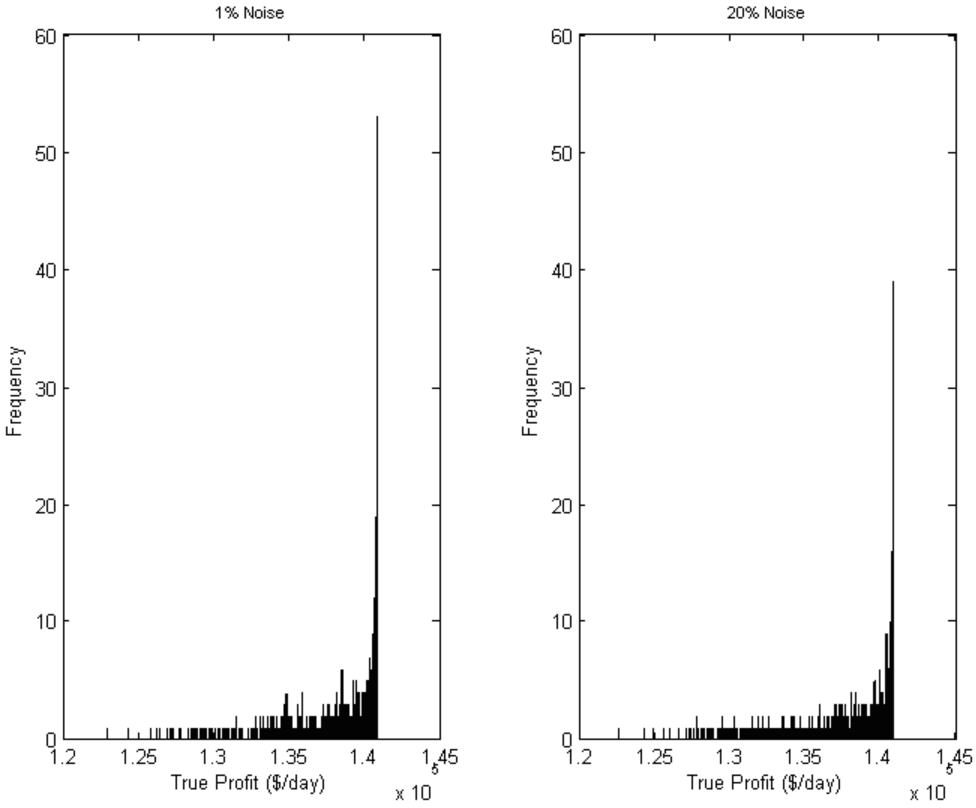

Figure 8.8. The effect of sensor noise on the variation of true profit for a tube temperature of 1415 K.

At first glance it appears that reducing the amount of sensor noise on the composition analyzers has a larger effect when the furnace tube temperature is assumed to be operated at 1200 K. However, a closer look reveals that this is not the case. Figures 8.5 and 8.7 show that the optimization curve is much steeper when the furnace tube temperature is assumed to be operated at 1415 K meaning that deviations in the calculated optimum dilution steam to hydrocarbon ratio result in a much more significant loss of profit.

CHAPTER 9

CONCLUSIONS AND RECCOMENDATIONS

9.1 Conclusions

It can be concluded from the results provided in this study that structural model mismatch between the process and the optimization models can be identified by looking at the distribution of the calculated model parameters over a range of operating conditions. When possible, it was shown that the distribution of the calculated model parameters increases as the degree of mismatch is increased. Furthermore, it has been shown that in order to identify the mismatch, the variation caused by the structural model mismatch must outweigh the variation caused by sensor noise.

This study has also shown that there is value in reducing the amount of sensor noise on sensors that are used by an optimization application. The increase in overall profit attained varies from process to process and in each case considered in this study the increase in profit was always less than 0.5% and more typically 0.004 to 0.4%. Using the ethylene furnace model it was shown that the increase in profit when sensor noise is reduced depends on the shape of the optimization curve. A sharper curve about the optimum leads to a larger increase in profit when sensor noise is reduced.

9.2 Recommendations

This study, for the most part, was conducted using simple process models. Future work should include industrial scale optimization models along with actual process data.

All cases considered in this study update only one or two parameters and optimize the process by manipulating one variable. Industrial optimization applications update many model parameters and are multidimensional optimization problems which should be taken into consideration in future work. The use of real process data and industrial optimization models will help to show the true value of this work in an industrial environment.

It was shown in this work that although the variation of the calculated model parameters can be used to identify structural model mismatch there is a limit to the amount of noise that allows for this identification. In almost every case excessive amounts of sensor noise prevent the identification of model mismatch. This leads to the question of how much sensor noise is allowable to identify structural model mismatch. As this question was considered it became clear that the problem is very complex. In order to be able to identify the structural mismatch the variation caused by the mismatch must outweigh the variation caused by sensor noise. While the variation caused by sensor noise can be found either stochastically or by taking the partial derivative of the model parameter with respect to each sensor and then summing the values it is much more difficult to determine the variation caused by model mismatch. The difficulty arises from the fact that not only is it hard to identify the variation caused by model mismatch but also that the variation depends on the magnitude of the variation in the process operating conditions. Future work should be focused on developing a procedure that can be used to determine the maximum amount of sensor noise that still allows for the identification of model mismatch.

The value of an improved measurement was considered in this study but there is much more to the problem than was considered here. The actual value of the improved measurement depends on the effect of the model parameter that is being calculated from the measurement on the optimum conditions of the process. If a model parameter has little effect on the optimum operating conditions of a process the sensors used to calculate that parameter will most likely be of little value. On the other hand, if the parameter has a large effect on the optimum then there will probably be significant value in using a better sensor. Future studies should look at the value of an improved measurement in a multidimensional optimization problem because sensor noise will probably have a larger effect when more than one variable is being used to optimize the process. A proper procedure should first look at the value of the parameter in which the measurement is being used to calculate and then determining the variation in that parameter caused by variations in the measurement.

The primary application of the methodology used in this work will most likely be as an RTO monitoring tool. RTO applications tend to perform well when initially commissioned but the performance usually deteriorates over time due to changes in the process. It is theorized that as the performance of the RTO application deteriorates there will be increased variation in the calculated model parameters. Historical data from an actual RTO application should be used to see how the variation of the calculated model parameters changes over time.

BIBLIOGRAPHY

Bagajewicz, M., and M. Markowski, and A. Budek. Economic Value of Precision in the Monitoring of Linear Systems. *Submited to AICHE Journal*, 2003.

Beautyman, A.C. Assessing Profitability of Real-Time Optimization. *Hydrocarbon Process.*, **83** (6), 2004, 39-42.

Bennett, C.O., and J.E. Myers. *Momentum, Heat, and Mass Transfer, 2nd ed.*, McGraw Hill, New York, 1974.

Biegler, L.T., and I.E. Grossman. Retrospective on Optimization. *Comput. Chem. Eng.*, **28**, 2004, 1169-1192.

Biegler, L.T., and I.E. Grossman. Part II. Future Perspective on Optimization. *Comput. Chem. Eng.*, **28**, 2004, 1193-1218.

Bischoff, K.B., and G.F. Froment. *Chemical Reactor Analysis and Design*. John Wiley & Sons Inc., New York, NY, 1990.

Bybee, K. Promoting Real-Time Optimization of Hydrocarbon-Producing Systems. *Journal of Petroleum Technology*, **55** (12), 2003, 34-35.

Casey, L.K., R.E. Galloway, A. Georgiou, A.V. Sapre, and P. Taylor. Ethylene Optimization System Reaps Operations and Maintenance Benefits. *Oil and Gas Journal*, **Mar. 9**, 1998, 46-50.

Cheng, J.H., and E. Zafiriou. Measurement Noise Tolerance and Results Analysis for Iterative Feedback Steady-State Optimization. *Ind. Eng. Chem. Res.*, **43**, 2004, 3577-3589.

Cheng, J.H., and E. Zafiriou. Robust Model-Based Iterative Feedback Optimization of Steady State Plant Operations. *Ind. Eng. Chem. Res.*, **39**, 2000, 4215-4227.

Finco, M.V. The Modeling and Control of Low Relative Volatility Splitters. M.S. Thesis, Lehigh University, Bethlehem, PA, 1987.

Forbes, J.F., L.M. Fraleigh, and M. Guay. Sensor Selection for Model-Based Real-Time Optimization: Relating Design of Experiments and Design Cost. *Journal of Process Control*, **13**, 2003, 667-678.

Forbes, J.F., T.E. Marlin, and J.F. MacGregor. Model Adequacy Requirements for Optimizing Plant Operations. *Comput. Chem. Eng.*, **18** (6), 1994, 497-510.

Forbes, J.F., A. Singh, P.J. Vermeer, and S.S. Woo. Model-Based Real-Time Optimization of Automotive Gasoline Blending Operations. *Journal of Process Control*, **10**, 2000, 43-58.

Froment, G.F., P.M. Plehiers, and G.C. Reyniers. Simulation of the Run Length of an Ethane Cracking Furnace. *Ind. Eng. Chem. Res.*, **29**, 1990, 636-641.

Froment, G.F., and K.M. Sundaram. Modeling of Thermal Cracking Kinetics. 3. Radical Mechanisms for the Pyrolysis of Simple Paraffins, Olefins, and Their Mixtures. *Ind. Eng. Chem. Fundam.*, **17** (3), 1978, 174-182.

Gao, L., and N.W. Loney. Evolutionary Polymorphic Neural Network in Chemical Process Modeling. *Comput. Chem. Eng.*, **25**, 2001, 1403-1410.

Gau, C.Y., and M.A. Stadtherr. New Interval Methodologies for Reliable Chemical Process Modeling. *Comput. Chem. Eng.*, **26**, 2002, 827-840.

Graells, M., M. Herrera, L. Puigjaner, and S.E. Sequeira. On-Line Process Optimization: Parameter Tuning for the Real Time Evolution (RTE) Approach. *Comput. Chem. Eng.*, **28**, 2004, 661-672.

Gupta, S.K., S.V. Inamdar, and D.N. Saraf. Multi-Objective Optimization of an Industrial Crude Distillation Unit Using the Elitist Non-Dominated Sorting Genetic Algorithm. *Chem. Eng. Res. Des.*, **82** (A5), 2004, 611-623.

Hurowitz, S.E. *Superfractionator Process Control*. Ph.D. Dissertation, Texas Tech University, Lubbock, TX, 1998.

Incropera, F.P., and D.P. DeWitt. *Fundamentals of Heat and Mass Transfer, 5th Edition.* John Wiley & Sons Inc., New York, NY, 2002.

Jutan, A., and Q. Xiong. Continuous Optimization Using a Dynamic Simplex Method. *Chem. Eng. Sci.*, **58**, 2003, 3817-3828.

Krishnan, S., G.W. Barton, and J.D. Perkins. Robust Parameter Estimation in On-Line Optimization-Part I. Methodology and Simulated Case Study. *Comput. Chem. Eng.*, **16**, 1992, 545-562.

Lauks, U.E., C. van Leeuwen, P.J. Valkenburg, and R.J. Vasbinder. On-Line Optimization of an Ethylene Plant. *Comput. Chem. Eng.*, **16**, 1992, S213-S220.

Maame, Y.B., L.T. Biegler, and J.D. Kelly. Nonlinear Optimization with Many Degrees Of Freedom in Process Engineering. *Ind. Eng. Chem.*, **43**, 2004, 6803-6812.

Mann, U. *Principles of Chemical Reactor Analysis and Design.* Plains Publishing Company, Lubbock, TX, 1999.

Marlin, T.E., and I.P. Miletic. Results Diagnosis for Real-Time Process Operations Optimization. *Comput. Chem. Eng.*, **22**, 1998, S475-S482.

Marlin, T.E., and W.S. Yip. Multiple Data Sets for Model Updating in Real-Time Operations Optimization. *Comput. Chem. Eng.*, **26**, 2002, 1345-1362.

Milectic, I.P. and T.E. Marlin. On-Line Statistical Results Analysis in Real-Time Operations Optimization. *Ind. Eng. Chem. Res.*, **37**, 1998, 3670-3684.

Palmer, K., and M. Realff. Metamodeling Approach to Optimization of Steady-State Flowsheet Simulations: Model Generation. *Trans IChemE*. **80**, 2002, 760-772.

Quesada, I., and I.E. Grossman. An LP/NLP Based Branch and Bound Algorithm for Convex MINLP Optimization Problems. *Comput. Chem. Eng.*, **16**, 1992, 937-947.

Rao, S.S. *Applied Numerical Methods for Engineers and Scientists*. Prentice Hall, Upper Saddle River, NJ, 2002.

Rico-Ramirez, V., and A.W. Westerberg. Structural Analysis of Conditional Models. *Comput. Chem. Eng.*, **26**, 2002, 359-373.

Riggs, J.B. *An Introduction to Numerical Methods for Chemical Engineers, 2nd Edition.* Texas Tech University Press, Lubbock, TX, 1994

Riggs, J.B. *Chemical Process Control, 2nd Edition.* Ferret Publishing, Lubbock, TX, 2001.

Sahinidis, N.V. Optimization Under Uncertainty: State-of-the-Art and Opportunities, *Comput. Chem. Eng.*, **28**, 2004, 971-983.

Sequeira, S.E., M. Graells, and L. Puigjaner. Real-Time Evolution for On-Line Optimization of Continuous Processes. *Ind. Eng. Chem. Res.*, **41**, 2002, 1815-1825.

Tsai, T.C., R. Zou, and J. Zou. Model Predicts Yields from Ethan-Propane Cocracking. *Oil and Gas Journal*, **Dec. 21**, 1987, 38-41.

Turton, R., R.C. Bailie, W.B. Whiting, and J.A. Shaeiwitz. *Analysis, Synthesis, and Design of Chemical Processes, 2nd Edition.* Prentice Hall, Upper Saddle River, NJ, 2003.

Wankat, P.C. *Separations in Chemical Engineering: Equilibrium Staged Separtations.* Prentice-Hall Inc., Upper Saddle River, NJ, 1988.

Westervelt, R. "ExxonMobil: Leading the Petchem Upturn." *Chemical Week.* November 24, 2004, 27.

Yan, M. *Simulation and Optimization of an Ethylene Plant*. Master's Thesis, Texas Tech University, Lubbock, TX, 2000.

Yip, W.S., and T.E. Marlin. The Effect of Model Fidelity on Real-Time Optimization Performance. *Comput. Chem. Eng.*, **28**, 2004, 267-280.

Zhang, Y., D. Moner, and J.F. Forbes. Real-Time Optimization Under Parametric Uncertainty: A Probability Constrained Approach. *Journal of Process Control*, **12**, 2002, 373-389.

APPENDIX A

REACTION NETWORK FOR COMPLEX AND SIMPLIFIED FURNACE MODELS

Table A.1 Complex furnace model reaction network and its kinetic data (Yan, 2000).

No	Reaction	A ($kcal/mole$)	E (sec^{-1} or $L/mole \cdot sec$)	Reaction Rate
1	$C_2H_6 \rightarrow 2CH_3\bullet$	4.0×10^{16}	87.5	$r_1=k_1[C_2H_6]$
2	$C_3H_8 \rightarrow C_2H_5\bullet + CH_3\bullet$	2.0×10^{16}	84.5	$r_2=k_2[C_3H_8]$
3	$n\text{-}C_4H_{10} \rightarrow 2C_2H_5\bullet$	1.5×10^{16}	82.1	$r_3=k_3[n\text{-}C_4H_{10}]$
4	$n\text{-}C_4H_{10} \rightarrow 1\text{-}C_3H_7\bullet + CH_3\bullet$	9.0×10^{16}	85.4	$r_4=k_4[n\text{-}C_4H_{10}]$
5	$1\text{-}C_4H_8 \rightarrow C_3H_5\bullet + CH_3\bullet$	8.0×10^{16}	74.0	$r_5=k_5[1\text{-}C_4H_8]$
6	$C_2H_4+H\bullet \rightarrow C_2H_3\bullet + H_2$	8.0×10^{8}	4.0	$r_6=k_6[C_2H_4][H\bullet]$
7	$C_2H_6+H\bullet \rightarrow C_2H_5\bullet + H_2$	1.0×10^{11}	9.7	$r_7=k_7[C_2H_6][H\bullet]$
8	$C_3H_6+H\bullet \rightarrow C_3H_5\bullet + H_2$	2.5×10^{9}	1.1	$r_8=k_8[C_3H_6][H\bullet]$
9	$C_3H_8+H\bullet \rightarrow 1\text{-}C_3H_7\bullet + H_2$	1.0×10^{11}	9.7	$r_9=k_9[C_3H_8][H\bullet]$
10	$C_3H_8+H\bullet \rightarrow 2\text{-}C_3H_7\bullet + H_2$	9.0×10^{10}	8.3	$r_{10}=k_{10}[C_3H_8][H\bullet]$
11	$1\text{-}C_4H_8+H\bullet \rightarrow C_4H_7\bullet + H_2$	5.0×10^{10}	3.9	$r_{11}=k_{11}[1\text{-}C_4H_8][H\bullet]$
12	$C_2H_4+CH_3\bullet \rightarrow C_2H_3\bullet + CH_4$	1.0×10^{10}	13.0	$r_{12}=k_{12}[C_2H_4][CH_3\bullet]$
13	$C_2H_6+CH_3\bullet \rightarrow C_2H_5\bullet + CH_4$	3.8×10^{11}	16.5	$r_{13}=k_{13}[C_2H_6][CH_3\bullet]$
14	$C_3H_6+CH_3\bullet \rightarrow C_3H_5\bullet + CH_4$	2.0×10^{9}	12.2	$r_{14}=k_{14}[C_3H_6][CH_3\bullet]$
15	$C_3H_8+CH_3\bullet \rightarrow 1\text{-}C_3H_7\bullet + CH_4$	3.4×10^{10}	11.5	$r_{15}=k_{15}[C_3H_8][CH_3\bullet]$

Table A.1 Continued

No	Reaction	A ($kcal/mole$)	E (sec^{-1} or $L/mole \cdot sec$)	Reaction Rate
16	$C_3H_8+CH_3\bullet \rightarrow 2\text{-}C_3H_7\bullet + CH_4$	4.0×10^9	10.1	$r_{16}=k_{16}[C_3H_8][CH_3\bullet]$
17	$1\text{-}C_4H_8+CH_3\bullet \rightarrow C_4H_7\bullet + CH_4$	1.0×10^8	7.3	$r_{17}=k_{17}[1\text{-}C_4H_8][CH_3\bullet]$
18	$C_3H_6+C_2H_3\bullet \rightarrow C_3H_5\bullet + C_2H_4$	3.0×10^9	14.5	$r_{18}=k_{18}[C_3H_6][C_2H_3\bullet]$
19	$C_3H_8+C_2H_3\bullet \rightarrow 1\text{-}C_3H_7\bullet + C_2H_4$	3.0×10^9	18.8	$r_{19}=k_{19}[C_3H_8][C_2H_3\bullet]$
20	$C_3H_8+C_2H_3\bullet \rightarrow 2\text{-}C_3H_7\bullet + C_2H_4$	1.0×10^9	16.2	$r_{20}=k_{20}[C_3H_8][C_2H_3\bullet]$
21	$C_2H_4+C_2H_5\bullet \rightarrow CH_3\bullet + C_3H_6$	3.0×10^9	19.0	$r_{21}=k_{21}[C_2H_4][C_2H_5\bullet]$
22	$C_3H_6+C_2H_5\bullet \rightarrow C_3H_5\bullet + C_2H_6$	1.0×10^8	9.2	$r_{22}=k_{22}[C_3H_6][C_2H_5\bullet]$
23	$C_3H_8+C_2H_5\bullet \rightarrow 1\text{-}C_3H_7\bullet + C_2H_6$	1.2×10^9	12.6	$r_{23}=k_{23}[C_3H_8][C_2H_5\bullet]$
24	$C_3H_8+C_2H_5\bullet \rightarrow 2\text{-}C_3H_7\bullet + C_2H_6$	8.0×10^8	10.4	$r_{24}=k_{24}[C_3H_8][C_2H_5\bullet]$
25	$C_3H_8+C_3H_5\bullet \rightarrow 1\text{-}C_3H_7\bullet + C_3H_6$	1.0×10^9	18.8	$r_{25}=k_{25}[C_3H_8][C_3H_5\bullet]$
26	$C_3H_8+C_3H_5\bullet \rightarrow 2\text{-}C_3H_7\bullet + C_3H_6$	8.0×10^8	16.2	$r_{26}=k_{26}[C_3H_8][C_3H_5\bullet]$
27	$C_2H_3\bullet \rightarrow C_2H_2 + H\bullet$	2.0×10^9	31.5	$r_{27}=k_{27}\,[C_2H_3\bullet]$
28	$C_2H_5\bullet \rightarrow C_2H_4 + H\bullet$	3.2×10^{13}	40.0	$r_{28}=k_{28}\,[C_2H_5\bullet]$
29	$C_3H_5\bullet \rightarrow C_2H_2 + CH_3\bullet$	3.0×10^{10}	36.2	$r_{29}=k_{29}\,[C_3H_5\bullet]$
30	$1\text{-}C_3H_7\bullet \rightarrow C_2H_4 + CH_3\bullet$	4.0×10^{13}	32.6	$r_{30}=k_{30}\,[1\text{-}C_3H_7\bullet]$

Table A.1 Continued

No	Reaction	A ($kcal/mole$)	E (sec^{-1} or $L/mole \cdot sec$)	Reaction Rate
31	$1\text{-}C_3H_7\bullet \rightarrow C_3H_6 + H\bullet$	2.0×10^{13}	34.8	$r_{31}=k_{31}\,[1\text{-}C_3H_7\bullet]$
32	$2\text{-}C_3H_7\bullet \rightarrow C_3H_6 + H\bullet$	2.0×10^{13}	38.7	$r_{32}=k_{32}\,[2\text{-}C_3H_7\bullet]$
33	$C_4H_7\bullet \rightarrow C_4H_6 + H\bullet$	1.2×10^{14}	49.3	$r_{33}=k_{33}\,[C_4H_7\bullet]$
34	$C_4H_7\bullet \rightarrow C_2H_4 + C_2H_3\bullet$	1.0×10^{11}	37.0	$r_{34}=k_{34}\,[C_4H_7\bullet]$
35	$1\text{-}C_4H_9\bullet \rightarrow C_2H_4 + C_2H_5\bullet$	1.6×10^{12}	28.0	$r_{35}=k_{35}\,[1\text{-}C_4H_9\bullet]$
36	$1\text{-}C_4H_9\bullet \rightarrow 1\text{-}C_4H_8 + H\bullet$	1.0×10^{13}	36.6	$r_{36}=k_{36}\,[1\text{-}C_4H_9\bullet]$
37	$2\text{-}C_4H_9\bullet \rightarrow C_3H_6 + CH_3\bullet$	2.5×10^{13}	31.9	$r_{37}=k_{37}\,[2\text{-}C_4H_9\bullet]$
38	$2\text{-}C_4H_9\bullet \rightarrow 1\text{-}C_4H_8 + H\bullet$	2.0×10^{13}	39.8	$r_{38}=k_{38}\,[2\text{-}C_4H_9\bullet]$
39	$C_5H_{11}\bullet \rightarrow C_5H_{10} + H\bullet$	5.0×10^{13}	36.6	$r_{39}=k_{39}\,[C_5H_{11}\bullet]$
40	$C_5H_{11}\bullet \rightarrow 1\text{-}C_4H_8 + CH_3\bullet$	3.2×10^{13}	31.5	$r_{40}=k_{40}\,[C_5H_{11}\bullet]$
41	$C_5H_{11}\bullet \rightarrow C_2H_4 + 1\text{-}C_3H_7\bullet$	4.0×10^{12}	28.7	$r_{41}=k_{41}\,[C_5H_{11}\bullet]$
42	$C_2H_2 + H\bullet \rightarrow C_2H_3\bullet$	4.0×10^{10}	1.3	$r_{42}=k_{42}[C_2H_2][H\bullet]$
43	$C_2H_4 + H\bullet \rightarrow C_2H_5\bullet$	1.0×10^{10}	1.5	$r_{43}=k_{43}[C_2H_4][H\bullet]$
44	$C_3H_6 + H\bullet \rightarrow 1\text{-}C_3H_7\bullet$	1.0×10^{10}	2.9	$r_{44}=k_{44}[C_3H_6][H\bullet]$
45	$C_3H_6 + H\bullet \rightarrow 2\text{-}C_3H_7\bullet$	1.0×10^{10}	1.5	$r_{45}=k_{45}[C_3H_6][H\bullet]$

Table A.1 Continued

No	Reaction	A ($kcal/mole$)	E (sec^{-1} or $L/mole \cdot sec$)	Reaction Rate
46	$C_4H_6+H\bullet \rightarrow C_4H_7\bullet$	4.0×10^{10}	1.3	$r_{46}=k_{46}[C_4H_6][H\bullet]$
47	$1\text{-}C_4H_8+H\bullet \rightarrow 2\text{-}C_4H_9\bullet$	1.0×10^{10}	1.2	$r_{47}=k_{47}[1\text{-}C_4H_8][H\bullet]$
48	$C_2H_4+CH_3\bullet \rightarrow 1\text{-}C_3H_7\bullet$	2.0×10^{8}	7.9	$r_{48}=k_{48}[C_2H_4][CH_3\bullet]$
49	$C_3H_6+CH_3\bullet \rightarrow 1\text{-}C_4H_9\bullet$	3.2×10^{8}	9.1	$r_{49}=k_{49}[C_3H_6][C_2H_3\bullet]$
50	$C_2H_4+C_2H_3\bullet \rightarrow C_4H_7\bullet$	5.0×10^{7}	7.0	$r_{50}=k_{50}[C_2H_4][C_2H_3\bullet]$
51	$C_2H_4+C_2H_5\bullet \rightarrow 1\text{-}C_4H_9\bullet$	1.5×10^{7}	7.6	$r_{51}=k_{51}[C_2H_4][C_2H_5\bullet]$
52	$C_3H_6+C_2H_5\bullet \rightarrow C_5H_{11}\bullet$	1.3×10^{7}	7.5	$r_{52}=k_{52}[C_3H_6][C_2H_5\bullet]$
53	$C_2H_4+1\text{-}C_3H_7\bullet \rightarrow C_5H_{11}\bullet$	2.0×10^{7}	7.4	$r_{53}=k_{53}[C_2H_4][1\text{-}C_3H_7\bullet]$
54	$C_2H_4+2\text{-}C_3H_7\bullet \rightarrow C_5H_{11}\bullet$	1.3×10^{7}	6.9	$r_{54}=k_{54}[C_2H_4][2\text{-}C_3H_7\bullet]$
55	$1\text{-}C_4H_9\bullet \rightarrow 2\text{-}C_4H_9\bullet$	5.2×10^{14}	41.0	$r_{55}=k_{55}[1\text{-}C_4H_9\bullet]$
56	$C_2H_3\bullet+H\bullet \rightarrow C_2H_4$	1.0×10^{10}	0	$r_{56}=k_{56}[C_2H_3\bullet][H\bullet]$
57	$C_2H_5\bullet+H\bullet \rightarrow C_2H_6$	4.0×10^{10}	0	$r_{57}=k_{57}[C_2H_5\bullet][H\bullet]$
58	$C_3H_5\bullet+H\bullet \rightarrow C_3H_6$	2.0×10^{10}	0	$r_{58}=k_{58}[C_3H_5\bullet][H\bullet]$
59	$1\text{-}C_3H_7\bullet+H\bullet \rightarrow C_3H_8$	1.0×10^{10}	0	$r_{59}=k_{59}[1\text{-}C_3H_7\bullet][H\bullet]$
60	$2\text{-}C_3H_7\bullet+H\bullet \rightarrow C_3H_8$	1.0×10^{10}	0	$r_{60}=k_{60}[2\text{-}C_3H_7\bullet][H\bullet]$

Table A.1 Continued

No	Reaction	A ($kcal/mole$)	E (sec^{-1} or $L/mole \cdot sec$)	Reaction Rate
61	$C_4H_7\bullet+H\bullet\rightarrow 1\text{-}C_4H_8$	2.0×10^{10}	0	$r_{61}=k_{61}[C_4H_7\bullet][H\bullet]$
62	$1\text{-}C_4H_9\bullet+H\bullet\rightarrow n\text{-}C_4H_{10}$	1.0×10^{10}	0	$r_{62}=k_{62}[1\text{-}C_4H_9\bullet][H\bullet]$
63	$2\text{-}C_4H_9\bullet+H\bullet\rightarrow n\text{-}C_4H_{10}$	1.0×10^{10}	0	$r_{63}=k_{63}[2\text{-}C_4H_9\bullet][H\bullet]$
64	$C_5H_{11}\bullet+H\bullet\rightarrow C_5H_{12}$	1.0×10^{10}	0	$r_{64}=k_{64}[C_5H_{11}\bullet][H\bullet]$
65	$CH_3\bullet+CH_3\bullet\rightarrow C_2H_6$	1.3×10^{10}	0	$r_{65}=k_{65}[CH_3\bullet][CH_3\bullet]$
66	$C_2H_5\bullet+CH_3\bullet\rightarrow C_3H_8$	3.2×10^{9}	0	$r_{66}=k_{66}[C_2H_5\bullet][CH_3\bullet]$
67	$C_3H_5\bullet+CH_3\bullet\rightarrow 1\text{-}C_4H_8$	3.2×10^{9}	0	$r_{67}=k_{67}[C_3H_5\bullet][CH_3\bullet]$
68	$1\text{-}C_3H_7\bullet+CH_3\bullet\rightarrow n\text{-}C_4H_{10}$	3.2×10^{9}	0	$r_{68}=k_{68}[1\text{-}C_3H_7\bullet][CH_3\bullet]$
69	$2\text{-}C_3H_7\bullet+CH_3\bullet\rightarrow n\text{-}C_4H_{10}$	3.2×10^{9}	0	$r_{69}=k_{69}[2\text{-}C_3H_7\bullet][CH_3\bullet]$
70	$C_4H_7\bullet+CH_3\bullet\rightarrow C_5^+$	3.2×10^{9}	0	$r_{70}=k_{70}[C_4H_7\bullet][CH_3\bullet]$
71	$C_2H_3\bullet+C_2H_3\bullet\rightarrow C_4H_6$	1.3×10^{10}	0	$r_{71}=k_{71}[C_2H_3\bullet][C_2H_3\bullet]$
72	$C_4H_7\bullet+C_2H_3\bullet\rightarrow C_5^+$	1.3×10^{10}	0	$r_{72}=k_{72}[C_4H_7\bullet][C_2H_3\bullet]$
73	$C_2H_5\bullet+C_2H_5\bullet\rightarrow n\text{-}C_4H_{10}$	4.0×10^{8}	0	$r_{73}=k_{73}[C_2H_5\bullet][C_2H_5\bullet]$
74	$C_2H_5\bullet+C_2H_5\bullet\rightarrow C_2H_4+ C_2H_6$	5.0×10^{7}	0	$r_{74}=k_{74}[C_2H_5\bullet][C_2H_5\bullet]$
75	$C_3H_5\bullet+C_2H_5\bullet\rightarrow C_5^+$	3.2×10^{9}	0	$r_{75}=k_{75}[C_3H_5\bullet][C_2H_5\bullet]$

Table A.1 Continued

No	Reaction	A ($kcal/mole$)	E (sec^{-1} or $L/mole \cdot sec$)	Reaction Rate
76	$1\text{-}C_3H_7\bullet+C_2H_5\bullet\rightarrow C_5^+$	8.0×10^8	0	$r_{76}=k_{76}[1\text{-}C_3H_7\bullet][C_2H_5\bullet]$
77	$2\text{-}C_3H_7\bullet+C_2H_5\bullet\rightarrow C_5^+$	8.0×10^8	0	$r_{77}=k_{77}[2\text{-}C_3H_7\bullet][C_2H_5\bullet]$
78	$C_4H_7\bullet+C_2H_5\bullet\rightarrow C_5^+$	3.2×10^9	0	$r_{78}=k_{78}[C_4H_7\bullet][C_2H_5\bullet]$
79	$C_3H_5\bullet+C_3H_5\bullet\rightarrow C_5^+$	3.2×10^9	0	$r_{79}=k_{79}[C_3H_5\bullet][C_3H_5\bullet]$
80	$C_4H_7\bullet+C_3H_5\bullet\rightarrow C_5^+$	1.3×10^{10}	0	$r_{80}=k_{80}[C_4H_7\bullet][C_3H_5\bullet]$
81	$C_4H_7\bullet+C_4H_7\bullet\rightarrow C_5^+$	3.2×10^9	0	$r_{81}=k_{81}[C_4H_7\bullet][C_4H_7\bullet]$
82	$C_2H_2\rightarrow 2C+H_2$	5.0×10^{12}	62.0	$r_{82}=k_{82}[C_2H_2]$

Table A.2 Simplified furnace model reaction network and its kinetic data.

No	Reaction	A ($kcal/mole$)	E (sec^{-1} or $L/mole \cdot sec$)	Reaction Rate
1	$C_2H_6 \rightarrow C_2H_2+2H_2$	8.267×10^{11}	52.22	$r_1=k_1[C_2H_6]^{0.31}$
2	$C_3H_8 \rightarrow C_3H_6+H_2$	1.745×10^{26}	82.39	$r_2=k_2[C_3H_8]^{4.17}$
3	$C_3H_8 \rightarrow C_2H_4+CH_4$	4.881×10^{24}	79.31	$r_3=k_3[C_3H_8]^{3.58}$
4	$C_2H_6 \rightarrow C_2H_4+H_2$	2.925×10^{24}	83.00	$r_4=k_4[C_2H_6]^{3.28}$
5	$C_2H_6+H_2 \rightarrow 2CH_4$	1.407×10^{18}	82.62	$r_5=k_5[C_2H_6]^{0.46}$
6	$2C_2H_4 \rightarrow C_4H_6+H_2$	8.011×10^{20}	103.62	$r_6=k_6[C_2H_4]^{2.5}$
7	$C_2H_2 \rightarrow 2C+H_2$	5.00×10^{15}	62.00	$r_7=k_7[C_2H_2]$
8	$C_2H_6+C_3H_6 \rightarrow C_5^+$	6.543×10^{14}	60.30	$r_8=k_8[C_3H_6]^{0.78}$

APPENDIX B

COMPLEX AND SIMPLIFED FURNACE MODEL COMPARISONS

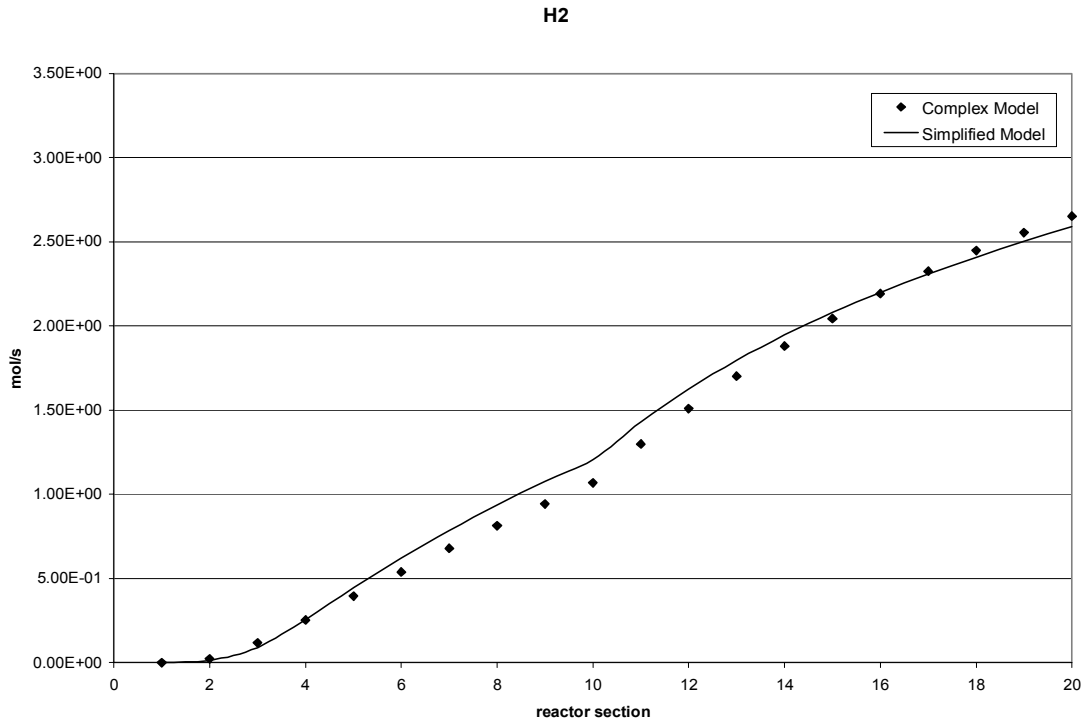

Figure B.1. H_2 flow rate comparison for the complex and simplified furnace models.

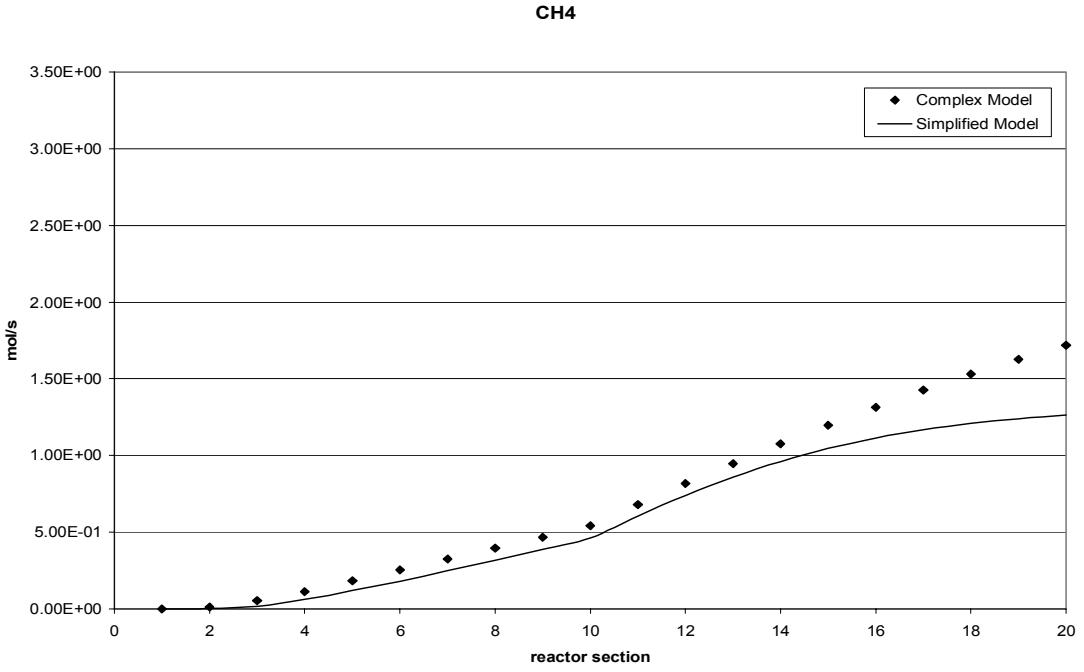

Figure B.2. CH_4 flow rate comparison for the complex and simplified furnace models.

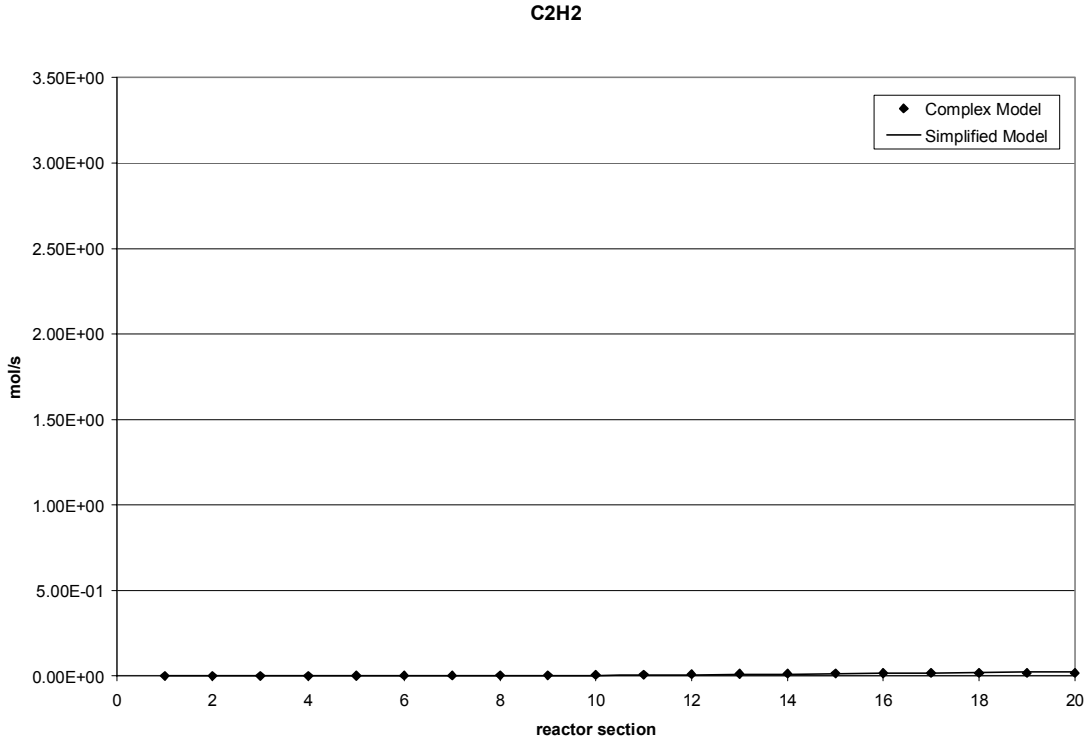

Figure B.3. C_2H_2 flow rate comparison for the complex and simplified furnace models.

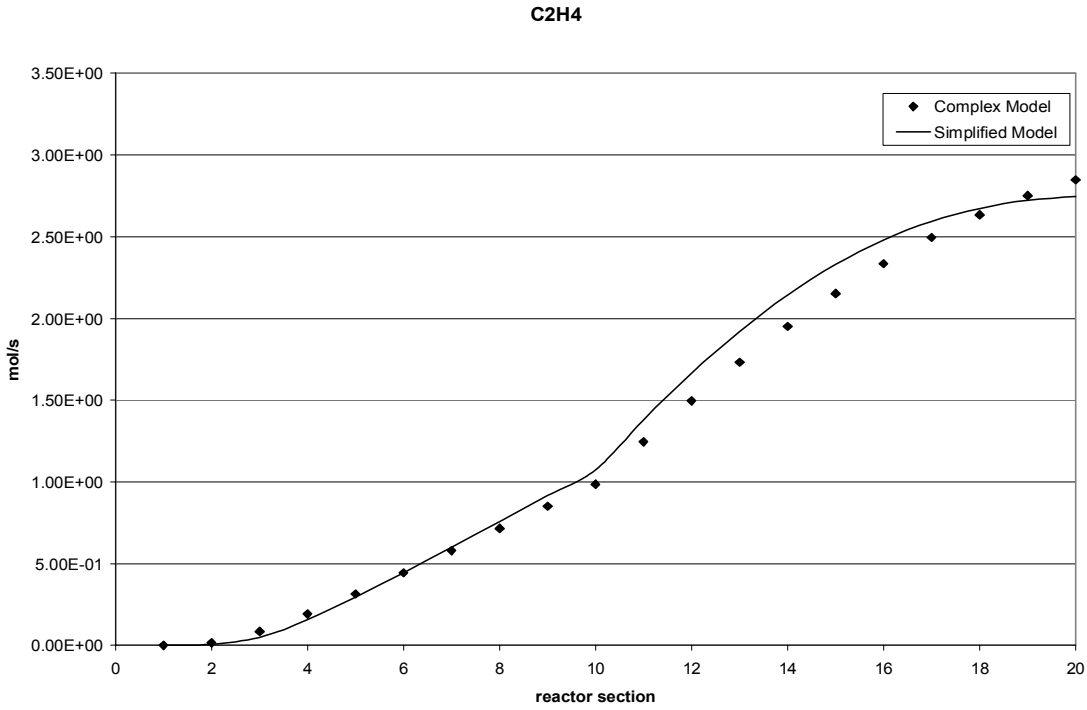

Figure B.4. C_2H_4 flow rate comparison for the complex and simplified furnace models.

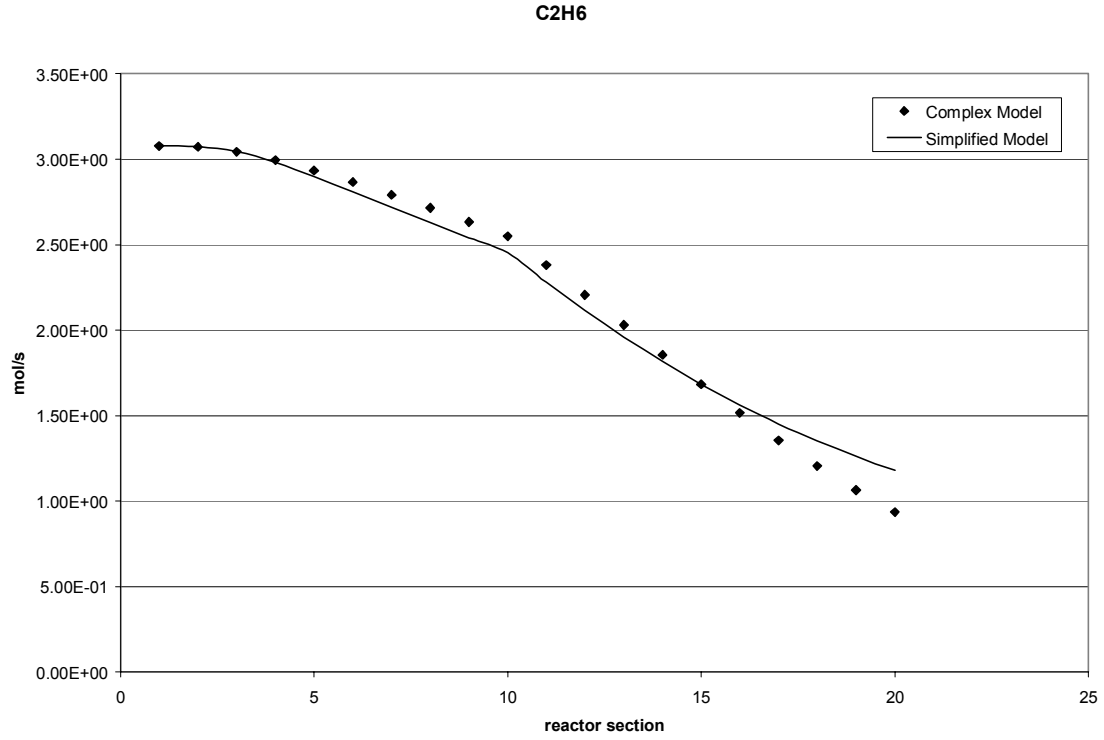

Figure B.5. C_2H_6 flow rate comparison for the complex and simplified furnace models.

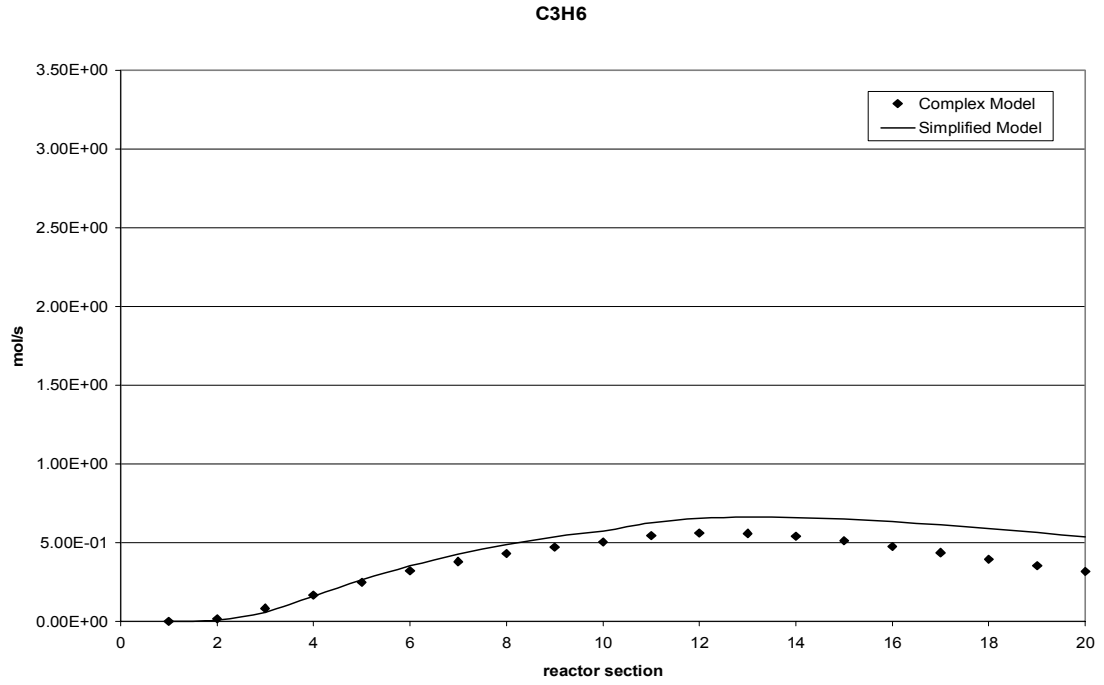

Figure B.6. C_3H_6 flow rate comparison for the complex and simplified furnace models.

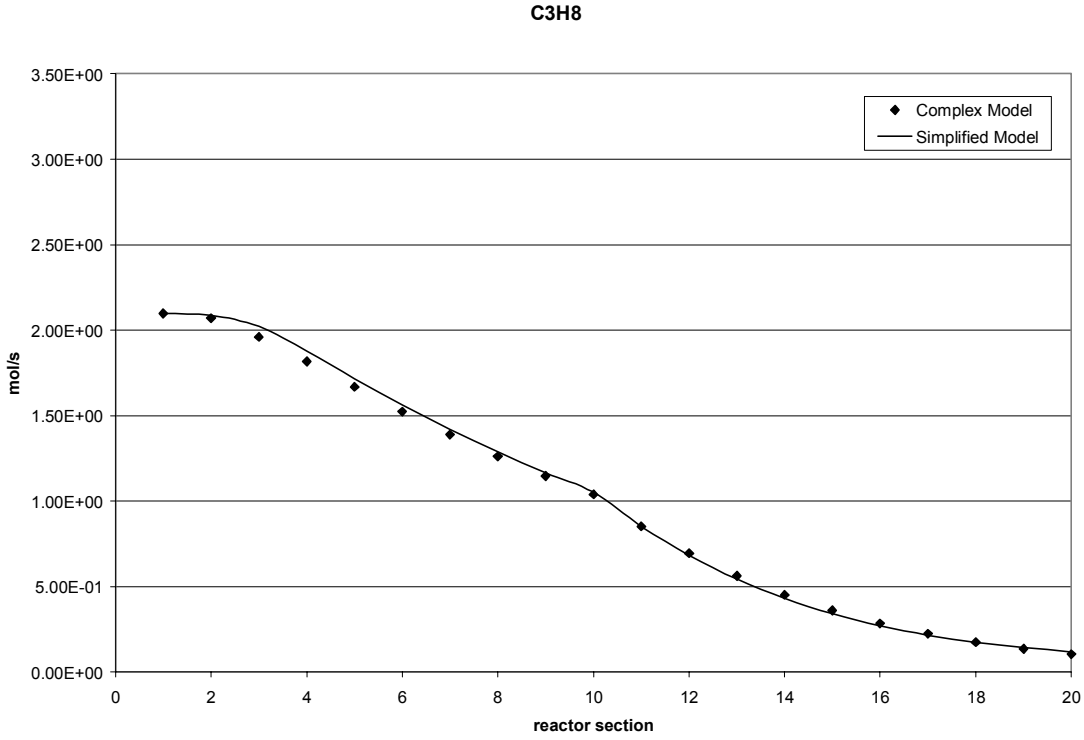

Figure B.7. C_3H_8 flow rate comparison for the complex and simplified furnace models.

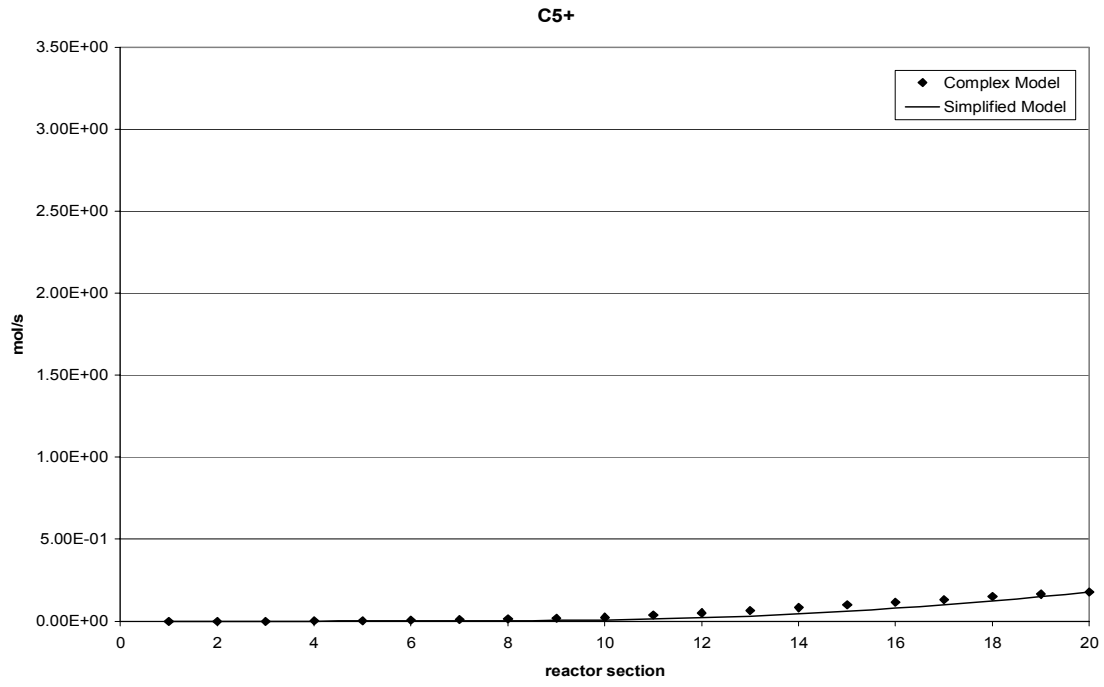

Figure B.8. C_5^+ flow rate comparison for the complex and simplified furnace models.

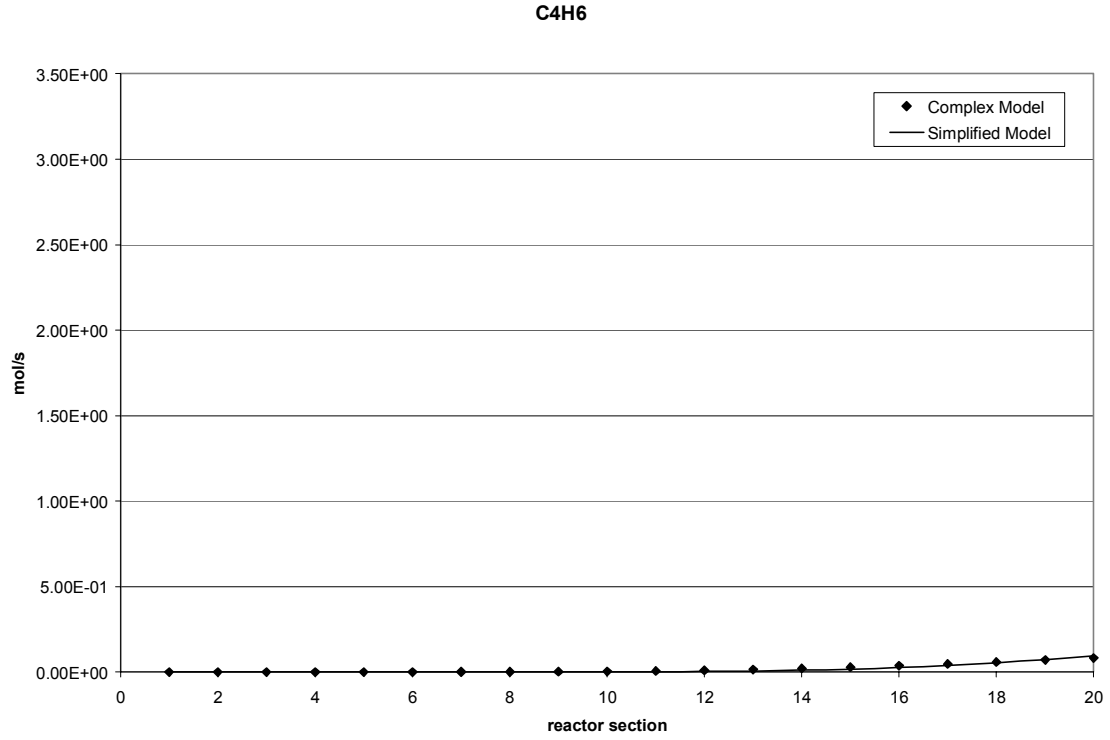

Figure B.9. C_4H_6 flow rate comparison for the complex and simplified furnace models.

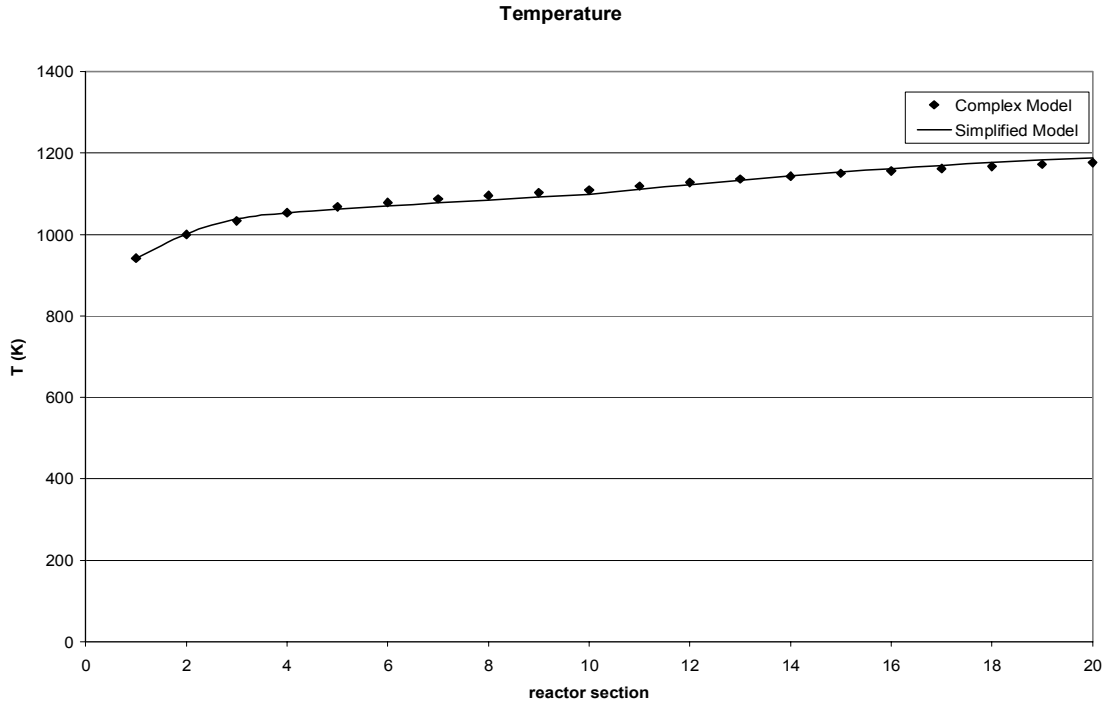

Figure B.10. Temperature comparison for the complex and simplified furnace models.

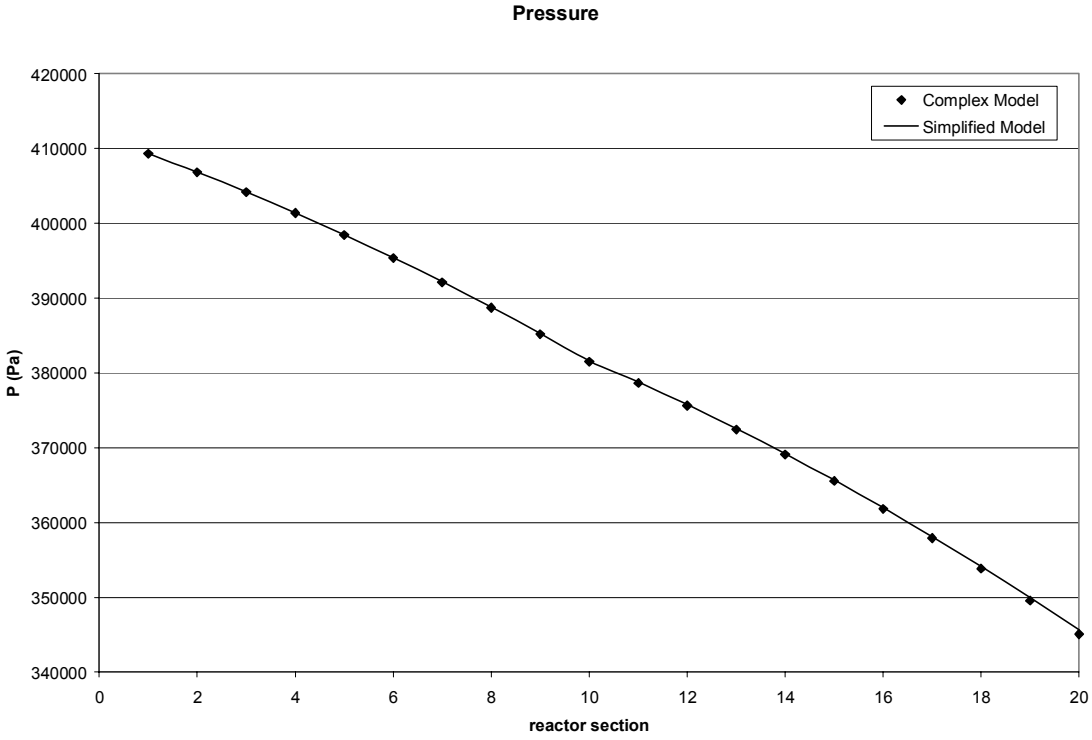

Figure B.11. Pressure comparison for the complex and simplified furnace models.

PERMISSION TO COPY

In presenting this thesis in partial fulfillment of the requirements for a master's degree at Texas Tech University or Texas Tech University Health Sciences Center, I agree that the Library and my major department shall make it freely available for research purposes. Permission to copy this thesis for scholarly purposes may be granted by the Director of the Library or my major professor. It is understood that any copying or publication of this thesis for financial gain shall not be allowed without my further written permission and that any user may be liable for copyright infringement.

Agree (Permission is granted.)

Jesse Saenz _____ _____
Student Signature Date

Disagree (Permission is not granted.)

_____ _____
Student Signature Date